UNIVERSIDAD DE INVESTIGACIÓN DE TECNOLOGÍA EXPERIMENTAL YACHAY

Escuela de Ciencias Químicas e Ingeniería

TÍTULO: PREPARATION AND CHARACTERIZATION OF MODIFIED-CELLULOSE SAMPLES OBTAINED FROM BIOMASS FOR POTENTIAL USE IN THE TOXIC METAL REMOVAL

Trabajo de integración curricular presentado como requisito para la obtención del título de Químico

Autor:

Saquinga Tirado Dayana Nathaly

Tutor:

Ph.D. López González Floralba

Co-Tutor:

MSc. De Lima Eljuri Lola María

Urcuquí, marzo del 2020

UNIVERSIDAD
YACHAY
TECH

Urcuquí, 26 de marzo de 2020

SECRETARÍA GENERAL
(Vicerrectorado Académico/Cancillería)
ESCUELA DE CIENCIAS QUÍMICAS E INGENIERÍA
CARRERA DE QUÍMICA
ACTA DE DEFENSA No. UITEY-CHE-2020-00014-AD

A los 26 días del mes de marzo de 2020, a las 15:00 horas, de manera virtual mediante videoconferencia, y ante el Tribunal Calificador, integrado por los docentes:

Presidente Tribunal de Defensa	Dra. VARELA SALAZAR, SOLMAR ALEXANDRA , Ph.D.
Miembro No Tutor	Dr. VILORIA VERA, DARIO ALFREDO , Ph.D.
Tutor	Dra. LOPEZ GONZALEZ, FLORALBA AGGENY , Ph.D.

El(la) señor(ita) estudiante **SAQUINGA TIRADO, DAYANA NATHALY**, con cédula de identidad No. **1804863668**, de la **ESCUELA DE CIENCIAS QUÍMICAS E INGENIERÍA**, de la Carrera de **QUÍMICA**, aprobada por el Consejo de Educación Superior (CES), mediante Resolución **RPC-SO-39-No.456-2014**, realiza a través de videoconferencia, la sustentación de su trabajo de titulación denominado: **REPARATION AND CHARACTERIZATION OF MODIFIED-CELLULOSE SAMPLES OBTAINED FROM BIOMASS FOR POTENTIAL USE IN THE TOXIC METAL REMOVAL**, previa a la obtención del título de **QUÍMICO/A**.

El citado trabajo de titulación, fue debidamente aprobado por el(los) docente(s):

Tutor	Dra. LOPEZ GONZALEZ, FLORALBA AGGENY , Ph.D.
Co - Tutor	Mgs. DE LIMA ELJURI, LOLA MARIA

Y recibió las observaciones de los otros miembros del Tribunal Calificador, las mismas que han sido incorporadas por el(la) estudiante.

Previamente cumplidos los requisitos legales y reglamentarios, el trabajo de titulación fue sustentado por el(la) estudiante y examinado por los miembros del Tribunal Calificador. Escuchada la sustentación del trabajo de titulación a través de videoconferencia, que integró la exposición de el(la) estudiante sobre el contenido de la misma y las preguntas formuladas por los miembros del Tribunal, se califica la sustentación del trabajo de titulación con las siguientes calificaciones:

Tipo	Docente	Calificación
Tutor	Dra. LOPEZ GONZALEZ, FLORALBA AGGENY , Ph.D.	10,0
Presidente Tribunal De Defensa	Dra. VARELA SALAZAR, SOLMAR ALEXANDRA , Ph.D.	10,0
Miembro Tribunal De Defensa	Dr. VILORIA VERA, DARIO ALFREDO , Ph.D.	10,0

Lo que da un promedio de: **10 (Diez punto Cero)**, sobre 10 (diez), equivalente a: **APROBADO**

Para constancia de lo actuado, firman los miembros del Tribunal Calificador, el/la estudiante y el/la secretario ad-hoc.

SAQUINGA TIRADO, DAYANA NATHALY
Estudiante

CERTIFICACIÓN ELECTRÓNICA
Firmado Digitalmente por: SOLMAR ALEXANDRA VARELA SALAZAR
Hora oficial Ecuador: 08/07/2020 12:36

Dra. VARELA SALAZAR, SOLMAR ALEXANDRA , Ph.D.
Presidente Tribunal de Defensa

FLORALBA AGGENY LOPEZ GONZALEZ

Dra. LOPEZ GONZALEZ, FLORALBA AGGENY , Ph.D.
Tutor

DARIO ALFREDO VILORIA VERA

Firmado digitalmente por DARIO ALFREDO VILORIA VERA
Fecha: 2020.07.09 17:28:59 -05'00'

Dr. VILORIA VERA, DARIO ALFREDO , Ph.D.
Miembro No Tutor

ESCOBAR LANDAZURI, ANA MARIA
Secretario Ad-hoc

ANA MARIA ESCOBAR LANDAZURI

AUTORÍA

Yo, **DAYANA NATHALY SAQUINGA TIRADO**, con cédula de identidad 104863668, declaro que las ideas, juicios, valoraciones, interpretaciones, consultas bibliográficas, definiciones y conceptualizaciones expuestas en el presente trabajo; así cómo, los procedimientos y herramientas utilizadas en la investigación, son de absoluta responsabilidad de el/la autora (a) del trabajo de integración curricular. Así mismo, me acojo a los reglamentos internos de la Universidad de Investigación de Tecnología Experimental Yachay.

Urcuquí, julio del 2020.

Dayana Saquinga

Dayana Nathaly Saquinga Tirado
CI: 1804863668

AUTORIZACIÓN DE PUBLICACIÓN

Yo, **DAYANA NATHALY SAQUINGA TIRADO,** con cédula de identidad 1804863668, cedo a la Universidad de Investigación de Tecnología Experimental Yachay, los derechos de publicación de la presente obra, sin que deba haber un reconocimiento económico por este concepto. Declaro además que el texto del presente trabajo de titulación no podrá ser cedido a ninguna empresa editorial para su publicación u otros fines, sin contar previamente con la autorización escrita de la Universidad.

Asimismo, autorizo a la Universidad que realice la digitalización y publicación de este trabajo de integración curricular en el repositorio virtual, de conformidad a lo dispuesto en el Art. 144 de la Ley Orgánica de Educación Superior

Urcuquí, julio del 2020.

Dayana Saquinga

Dayana Nathaly Saquinga Tirado
CI: 1804863668

Dedicatoria

Dedico mi trabajo a mis padres, Jesús y Elena, quienes han sido el pilar fundamental tanto para mi desarrollo personal como académico. A mi hermano Anthony, mi persona favorita, quien es el motor que me impulsa a ser mejor cada día, a Martha, Matilde y Walter por su amor y cuidado. Finalmente, a toda mi familia por sus consejos y apoyo incondicional en cada decisión que he tomado.

Dayana Nathaly Saquinga Tirado

Agradecimiento

Doy gracias a Dios por ser un amigo incondicional y por cuidarme, a mi familia y amigos por estar conmigo en momentos de alegría y tristeza. Agradezco a mis maestros de la Universidad Yachay Tech por el conocimiento proporcionado, la dedicación y los consejos. Un agradecimiento especial a mi tutora Floralba López y co-tutora Lola De Lima por su arduo trabajo y su enorme contribución al desarrollo de la investigación. Finalmente, agradezco a todos los miembros de TecnoEco que pertenecen al Centro Nacional de Investigaciones Metalúrgicas, a los maestros Carlos Reinoso y Edward Ávila de Yachay Tech por su valiosa contribución en la caracterización del material.

Dayana Nathaly Saquinga Tirado

Abbreviations

CRT: Cellulose from rose stem extracted with Toluene: Ethanol.

CRA$_2$: Cellulose from rose steam extracted with Nitric Acid/ Acetic Acid.

CRA$_2$F: Cellulose from rose extracted with Nitric Acid/ Acetic Acid, modified.

CS: Standard Cellulose.

PR: Precursor of the rose stem.

FT-IR: Fourier Transform Infrared Spectroscopy

NMR: Nuclear Magnetic Resonance

CP/MAS: Cross-Polarization Magic Angle Spinning

HPD: High-Power Decoupling

XPS: X-ray Photoelectron Spectroscopy

XRD: X-ray Diffraction

TGA: Thermogravimetric Analysis

C6: Carbo six (attribute to cellulose).

LoD: Limit of detection

LoQ: Limit of quantitation

N.S.: No Specification

Content

FIGURE INDEX

TABLE INDEX

RESUMEN

Las rosas son un producto que se encuentra en grandes cantidades en Ecuador, sus tallos se consideran un desecho agrícola, cuyo potencial no ha sido aprovechado. Para agregar valor a estos desechos, se extrae celulosa de ellos, con el fin de fabricar adsorbentes de bajo costo y respetuosos con el medio ambiente para la eliminación de Ni (II). Una vez que se recogieron los tallos de las rosas, se lavaron, se molieron y se tamizaron, se aplicaron dos métodos de extracción diferentes, el primero en condiciones básicas y el segundo en condiciones ácidas, obteniendo CRT y CRA_2, respectivamente. La muestra elegida para realizar análisis más profundos fue CRA_2, la misma que se acetiló en el proceso de extracción. Se aplicaron diferentes técnicas de caracterización a los sólidos obtenidos, tales como FT-IR, SEM, ^{13}C NMR, TGA, XRD y XPS. Los diferentes análisis mostraron que pequeñas cantidades de lignina y hemicelulosa no se eliminaron por completo en ambas muestras, así como también se confirmó la esterificación de CRA_2. La posterior modificación química con tiourea generó la muestra CRA_2F, que se corroboró mediante los análisis de la caracterización. Además, las pruebas de adsorción se llevaron a cabo variando la masa del adsorbente y manteniendo constante la cantidad de Ni (II) en solución. La cuantificación de níquel en solución requirió la formación de un complejo soluble de Ni (IV) con dimetilglioxima (dmgH2), para obtener límites de detección bajos que permitieran medir la concentración de níquel mediante espectroscopía UV-Vis. Finalmente, los modelos de Langmuir y Freundlich se ajustaron a los datos obtenidos para la adsorción de níquel en las muestras CRA_2 y CRA_2F, lo que resultó en un mejor ajuste para el modelo Freundlich. Sin embargo, según los análisis de XPS, no se ha descartado que se esté produciendo quimisorción en la superficie de las muestras de celulosa extraídas y modificadas.

Palabras clave: *celulosa, bio adsorbente, adsorción, desechos agrícolas, eliminación de níquel.*

ABSTRACT

Roses are a product that is found in large quantities in Ecuador, their stems are considered an agricultural waste, whose potential has not been harnessed. To add value to these wastes, cellulose is extracted from them, in order to manufacture low cost and environmentally friendly adsorbents for the Ni(II) removal. Once rose stems were recollected, washed, grounded and sieving two different extraction methods were applied, the first under a basic condition and the second using an acidic one, obtaining CRT and CRA_2, respectively. The sample chosen for conducting deeper analyzes was CRA_2, which was acetylated in the extraction process. Different characterization techniques were applied to the obtained solids such as FT-IR, SEM, ^{13}C NMR, TGA, XRD, and XPS. The different analyses showed that small amounts of lignin and hemicellulose have not been completely removed in both samples as well as the esterification of CRA_2 was confirmed. The subsequent chemical modification using thiourea generated the CRA_2F sample, which was corroborated by characterization analyses. In addition, the adsorption tests were carried out varying the mass of the adsorbent and keeping constant the amount of Ni(II) in solution. The quantification of nickel in solution required the formation of a soluble Ni(IV) complex with dimethylglyoxime (dmgH2), in order to obtain low detection limits allowing nickel concentration to be measured by UV-Vis spectroscopy. Finally, the models of Langmuir and Freundlich were fitted to the obtained data for the nickel adsorption on CRA_2 and CRA_2F samples, resulting in a better fit for the Freundlich model. However, according to XPS analyses, it has not been ruled out that chemisorption is occurring on the surface of extracted and modified cellulose samples.

Keywords: *Cellulose, bio adsorbent, adsorption, agricultural wastes, nickel removal.*

INTRODUCTION- JUSTIFICATION

Anthropogenic activities over the years have caused an increase in pollutants, largely affecting the bodies of water[1]. The elements commonly classified as "potentially toxic metals" include Zn, Pb, Hg, Cd, Ni, Cu, Cr, whose presence is involved in activities related to the development of society, having associated pollution and toxicity problems. Their concentration is increasing, mostly due to the activities of industrial or mining origin[2], such is the case of Nickel which is usually found in textile, battery manufacturing, and mineral processing industries[3]. Therefore, the design and implementation of a method for the effective recovery of these elements are necessary.

Methods based on the adsorption process have been shown to be a very convenient way to treat industrial effluents, due to advantages such as easiness of the developed procedure and the separation process involved, effectiveness and low cost. When adsorbents come from natural sources, these methods represent an ideal option for the recovery of potentially toxic elements, because the advantages of the high availability of the raw materials as well as the low environmental impact are added, which contribute to the protection of the environment[4]. In order to develop biomass-based adsorbents, biopolymers present in nature are exploited, being ecological and economical systems with very convenient properties. Among these biopolymers, polysaccharides are widely used being cellulose an important representative example.

Cellulose is the most abundant natural polymer on earth and it is the main component of the cell wall of plants[5]. This polysaccharide is formed by D-glucopyranose repeating units, linked by ß-1,4-glycosidic bonds[6]. This linear homopolymer has a high molecular, its linearity makes possible the construction of fibers that have high resistance[7]. According to literature, cellulose itself does not have a good adsorption capacity and physical stability[8], therefore it is convenient to carry out chemical modification, copolymerization, or crosslinking processes on it to achieve the more efficient system, improving its adsorption capacity, ion-exchange capacity as well as other properties[9].

The source of cellulose for this research project is the rose stems, these are obtained locally, in the north of Ecuador. Industries dedicated to the cultivation of flowers in Ecuador produce a great number of roses that due to their quality (thickness, extension) and beauty have been acquiring a worldwide recognition[10]. Wastes generated by rose crops industry make an important contribution to the total potential usable agricultural wastes, for which a particular use has not been conceived, beyond a fertilizer for later crops. For example, rose stems have not received adequate treatment and its potential has not been exploited. By means of this research project, it is proposed an alternative route for adding value to these agricultural wastes, taking advantage and revaluing the biomass present in them, for the preparation of adsorbents solids useful for the metal toxic removal.

Pre-treatment procedures for agricultural wastes are needed. For example, prior to use, the different raw material must be washed, dried, ground and sieved. Subsequently, the adsorbent precursor from the rose stems is subjected to different treatments for the extraction of cellulose[14,15], for which it was required a distinguishable and unambiguous sample codification. Furthermore, the modification of cellulose was made using thiourea[5] in order to improve the adsorption capacity of it and to obtain a better low-cost adsorbent. In addition, the adsorption data were analyzed by Langmuir and Freundlich models to evaluate the mechanism of the adsorption process.

The adsorption capacity of the adsorbents was evaluated by using UV-Vis spectroscopy. Structural and chemical characterization of the obtained solids, before and after of the modification, was carried out using Fourier Transform Infrared Spectroscopy (FTIR), ^{13}C Nuclear Magnetic Resonance (CP-MAS and HPD ^{13}C NMR), X-ray Photoelectron Spectroscopy (XPS), X-ray diffraction (XRD), and Scanning Electron Microscopy (SEM). Once developed the adsorption process, the surface was analyzed by XPS.

The present work has been divided into four chapters. In the first chapter, the Theoretical Framework is found, in which the information of precursor for the development of the adsorbents, the techniques employed and various important definitions are shown. The second chapter corresponds to the Experimental Section where each of the procedures used in the obtaining cellulose, solution preparation, adsorption processes are detailed. In the third chapter are the Results obtained with its respective interpretation and Discussion. Finally, the fourth chapter shows the Conclusions, and Recommendations for future research.

PROBLEM STATEMENT

The presence of potentially toxic metals in water bodies due to the different anthropogenic activities has caused concern regarding the contamination of the environment. Some of these activities, such as in the leather tanning, textile dyeing, and mineral processing involve the use of species of nickel that finally are released to the industrial effluents. If such effluents do not receive proper treatment, the nickel species will cause serious problems if its concentration exceeds a particular value. Therefore, proper treatment of the industrial effluents is necessary, and a more convenient method would be one that involves waste materials, which allows the removal and recovery of metals implying low cost and low environmental impact[11].

It has been proved that the use of natural adsorbents for the removal of toxic metals is a good option since, besides being friendly to the environment, their precursors are widely available in nature[12]. Rose crops are very important in Ecuador, and after their harvests, their stems are considered agricultural waste, without adequately to exploit their potential applicability. With the purpose to harness the biomass present in these agricultural wastes, it is suggested to carry out the manufacture of cellulose-based adsorbents. It is well known that cellulose is considered the most abundant natural polymer, and it can be extracted from renewable sources of biomass, such as wastes of rose crops, and from that, it is possible to prepare adsorbents with the capacity of toxic metal removal.

OBJECTIVES

General Objective

Preparation and characterization of cellulose-based adsorbents from biomass of agricultural wastes, such as rose stems, for the nickel removal present in aqueous solutions.

Specific Objectives

- Extract cellulose through acid and alkaline treatments using rose stems grounded as precursors.
- Modify cellulose structure through a simple method using an organosulfur compound such as thiourea.
- Provide added value to sources of biomass of agricultural wastes, such rose stems, with the development of adsorbents for the removal of potentially toxic metals, such as nickel, evaluating its adsorption capacity and efficiency.
- Characterize the surface of the adsorbent before and after the adsorption process using different techniques.

CHAPTER I

THEORETICAL FRAMEWORK

1.1 Floricultural Industry in Ecuador

Ecuador is one of the countries that has managed to position itself in the market as one of the main flower exporting countries. According to the National Association of Producers and Exporters of Flowers of Ecuador (Expoflores), the most exported flowers are roses with 76%, followed by summer flowers with 10%, gypsophila with 7%, lilies with 2% and carnation with 1%, the rest occupies 4%[13], having as main export markets for roses countries such as the United States, the European Union, Russia, among others[13]. In the markets of the different cities of Ecuador, there are varieties of flowers, in which the roses stand out, many of the time its long stems are cut, and then discarded, wasting its potential.

1.2 Cellulose, Hemicellulose and Lignin content in precursors

The percentages of lignocellulosic compounds in the precursor will depend on several factors such as the species of the plant, the age, the specific part of the plant and the growth conditions[14]. **Table 1** shows the ideal percentages of cellulose, hemicellulose, and lignin present in the rose stems.

Table 1 Cellulose, Hemicellulose and Lignin content of different raw materials.

Materials	Cellulose (%)	Hemicellulose (%)	Lignin (%)
Softwoods	38-46	23-31	22-34
Hardwoods	38-49	20-40	16-30
Straw	28-42	23-38	12-21
Bamboo	26-43	25-26	20-32
Cotton	80-85	n.d	n.d.
Corn cobs	18-40	11.34-31	14-19
Carnation stem	40-50	25-45	20-25
Pineaple crown	11-45	14-50	10-30
Rose stem	45-50	20-25	20-25
Orange peel	16.2	13.8	1
Corn stalk	50	20	30
Banana bagasse	55-65	14	11.58

Source: Adapted from González, K.-D, et al, (2016). Luna Azul ISSN 1909-2474, 43, 499–517.[15].

1.3 Cellulose

Cellulose is a biopolymer with impressive characteristics, it is mainly present in the plant cell wall and is responsible for the mechanical resistance of plants, although certain bacteria, algae, and fungi produce cellulose[16]. It is a non-branched homopolysaccharide formed by D-glucose units linked by glycosidic bonds (ß-1,4), showed in **Figure 1-A**, which consists of 10,000 to 15,000 units of D-glucose approximately[17]. In addition, this biopolymer forms a composite material with other polysaccharides, such as lignin and hemicellulose; their proportion in the plant cell wall will depend on the type of plant, and other factors[16,18].

Each of these constituents may be isolated by different chemical extraction, separation, and purification processes, due to the structural differences. For example, lignin is a cross-linked amorphous polymer that acts as a glue to hold the fibers in place, it is composed of three types of substituted phenols that are: sinapyl, coniferil, and p-coumaryl alcohols[19]. Hemicellulose is a branched heteropolymer, composed of different sugar monomers such as glucose, galactose, mannose, fructose, etc. This polymer, cellulose, and lignin contribute to strengthening the cell wall[20].

Cellulose has a semi-crystalline structure, that is, it is composed of crystalline and amorphous areas. The crystalline form of cellulose is due to the extensive hydrogen bonds, as it is represented in **Figure 1-B,** this can be affected by the source of cellulose and the methods used for its isolation, generally, the degree of crystallinity is in the range of 40 to 70%[18]. Cellulose can exist in four different polymorphs, called cellulose I, II, III, IV. The most common way to find it is as cellulose I or also called native cellulose, types II, III, IV are obtained after treatments with specific reagents[21]. Due to the broad chemical modifying capacity, and the formation of semicrystalline fibers Cellulose has been used in a wide variety of fields, one of the most important is in papermaking, but also is involved in fields related to the biomedical industry, biocomposites manufacture, wastewater remediation, among others[22].

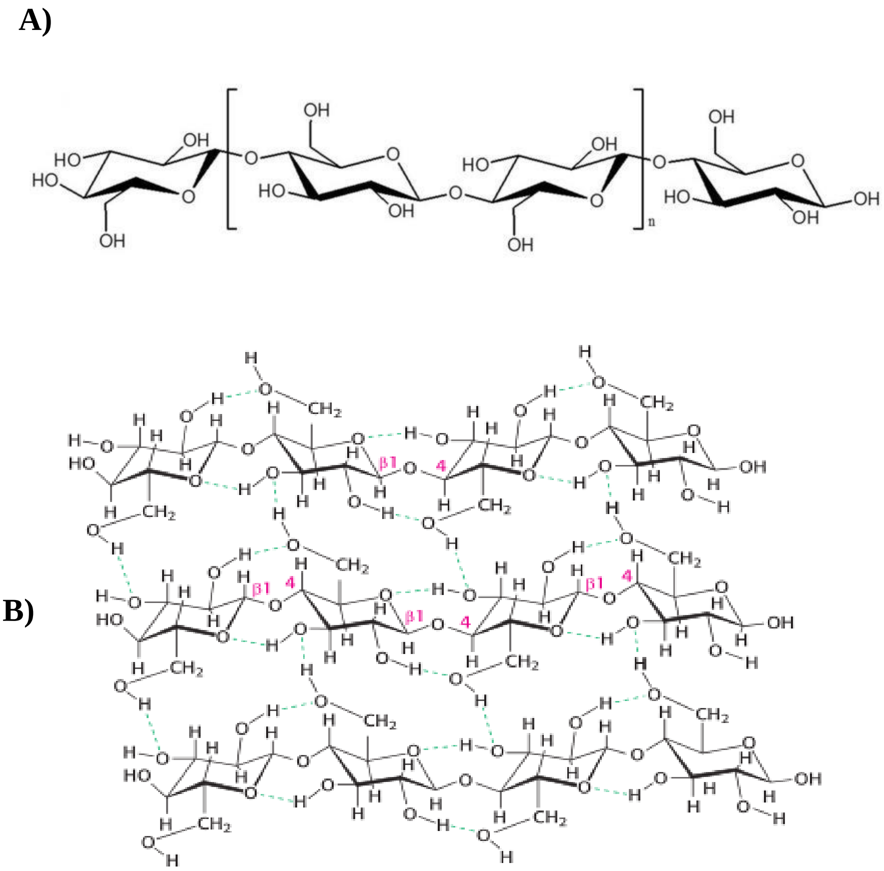

Figure 1 A) The β-1,4 linkages of Cellulose, they favor straight chains. **B)** Repetitive unit of cellulose.

Sources: **A.** Adapted from Kabir, F, et al (2018), Progress in Polymers, 153–174[6]. **B.** Adapted from Berg, J., et al (2007), *Biochemistry*, 1-1224 [6]

1.3.1 Reactivity of Cellulose

Cellulose has the capacity to participate in different chemical reactions, each anhydroglucose unit has hydroxyl groups, which are primary and secondary alcohols, located in the C-6, C-2, and C-3 carbons respectively. They are in equatorial positions and they are considered susceptible groups to chemical modification; hydrogens associated with these carbons are in axial position[23,24]. The substitution on the oxygen associated with the primary alcohol at C-6 is more thermodynamically favorable than on those associated with secondary alcohols at C-2 and C-3[25]. According to literature pure cellulose doesn't have a good adsorption capacity, due to this, it is necessary to make chemical modifications that allow it to increase its efficiency and achieve a better adsorption capacity.

A convenient treatment of functionalization or chemical modification would improve the efficiency of resulting based cellulose-adsorbents for metal ions removal, being also able to carry out multiple reuses to improve its applicability on a large scale[9,22]. Cellulose can be subject to copolymerization or cross-linking, oxidation, halogenation, esterification, and etherification, and other chemical modifications that make cellulose has new properties, thermal resistance or adsorption capacity enhancement[2,22]. A compound used for chemical modification of cellulose is thiourea, it is an organo-sulfur compound of formula $SC(NH_2)_2$, that is similar to urea but the properties of both differ significantly. It can also exist in its thiol form, called isothourea[26], as it can see in **Figure 2**.

This white crystalline solid is used in the textile, pharmaceutical industry, in the leaching of minerals, as a vulcanization accelerator, in the production of pesticides and as an auxiliary agent in diazo paper[27]. Sulfur-based compounds such as thiocarbonyl, thioethers, and thiols are widely studied for the adsorption of metals because they show an affinity towards them[28].

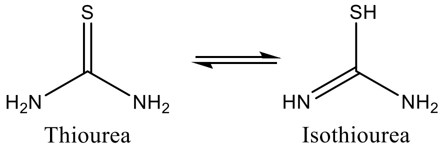

Figure 2 Tautomeric forms of thiourea

1.4 Nickel as a potentially toxic metal

Nickel is a chemical element with symbol Ni, of atomic number 28, it is located in group 10 and period IV of the periodic table, with electronic configuration $[Ar]\ 3d^8 4s^2$. Ni(II) is usually found together with other metals such as Cd, Zn, and Co in wastewater from the textile, tannery, battery manufacturing, automotive, mineral processing industries[3,29], etc. In addition, the use of nickel-plated components for the coating of pipes and connectors is directly related to the presence of significant amounts of nickel in the drinking water, exceeding the maximum allowed limits[30]. Depending on the exposure period, and the concentration, nickel can cause damage to health and contaminate the aquatic environment. Furthermore, certain nickel compounds such as $NiSO_4$, $NiCl_2$, $NiCO_3$ have been classified as carcinogenic[31,32]. One of the efficient and economical methods for the removal and recovery of nickel and other metals is by adsorption process, which is why the interest in the design and development of adsorbents from biomass has been increasing[3].

According to the Ecuadorian Institute for Normalization (INEN), the Ecuadorian Technical Standard (NTE INEN 1108) establishes requirements that drinking water must meet for human consumption[33]. Among these requirements are the maximum concentration limit (MCL) values allowed for some potentially toxic metals, such as nickel, cadmium, chromium, etc., and other chemical compounds, which are detailed in **Table 2**:

Table 2 Physical characteristics, inorganic substances and maximum limits allowed.

Parameter	**Unit**	**Maximum limit permitted**
Physical characteristics		
Color	Apparent color units (Pt-Co)	15
Turbidity	NTU	5
Odor	---	N.A
Flavor	---	N.A
Inorganic		
Antimony Sb	mg/L	0,02
Arsenic, As	mg/L	0,01
Barium, Ba	mg/L	0,7
Boron, B	mg/L	2,4
Cadmium, Cd	mg/L	0,003
Cyanides, CN^-	mg/L	0,07
Copper, Cu	mg/L	2,0
Chrome, Cr (cromo total)	mg/L	0,05
Fluorides	mg/L	1,5
Mercury, Hg	mg/L	0,006
Nickel, Ni	mg/L	0,07
Lead, Pb	mg/L	0,01
Selenium, Se	mg/L	0,04

Source: Adapted from INEN. *Norma Técnica Ecuatoriana - Agua Potable.* 2014, 1–10[33].

Other bibliographic sources that refer to these drinking water requirements, is given by the Environmental Quality and Effluent Discharge Standard: Water resource, available in Annex 1 of book VI of the Texto Unificado De Legislación Secundaria Del Ministerio Del Ambiente of Ecuador. This document establishes the permissible limits for discharges into large bodies of water or in water systems sewerage[34], which are specified in **Table 3** and **Table 4**.

Table 3 Water quality criteria for agricultural use in irrigation

Parameter	Expressed as	Unit	Quality criteria
Aluminum	Al	mg/L	5,0
Arsenic	As	mg/L	0,1
Beryllium	Be	mg/L	0,1
Boron	B	mg/L	0,75
Cadmium	Cd	mg/L	0,05
Zinc	Zn	mg/L	2,0
Cobalt	Co	mg/L	0,01
Copper	Cu	mg/L	0,2
Chrome	Cr^{+6}	mg/L	0,1
Fluorine	F	mg/L	1,0
Iron	Fe	mg/L	5,0
Lithium	Li	mg/L	2,5
Mercury	Hg	mg/L	0,001
Manganese	Mn	mg/L	0,2
Molybdenum	Mo	mg/L	0,01
Nickel	Ni	mg/L	0,2
pH	pH		6-9
Lead	Pb	mg/L	5,0
Selenium	Se	mg/L	0,02
Vanadium	V	mg/L	0,1

Source: Adapted from Ministerio del Ambiente (2014). *Anexo 1 Del Libro Vi Del Texto Unificado De Legislacion Secundaria Del Ministerio Del Ambiente.*, 1-40[33].

Table 4 Discharge limits to the public sewer system.

Parameters	Expressed as	Unit	Maximum limit permissible
Cadmium	Cd	mg/L	0,02
Total Cyanide	CN^-	mg/L	1,0
Zinc	Zn	mg/L	10,0
Total Cobalt	Co	mg/L	0,5
Copper	Cu	mg/L	1,0
Total Hydrocarbons of Petroleum	TPH	mg/L	20,0
Total Iron	Fe	mg/L	25,0
Total Manganese	Mn	mg/L	10,0
Mercury (total)	Hg	mg/L	0,01
Nickel	Ni	mg/L	2,0
Silver	Ag	mg/L	0,5
Lead	Pb	mg/L	0,5
Selenium	Se	mg/L	0,5

Source: Adapted from Ministerio del Ambiente (2014). *Anexo 1 Del Libro Vi Del Texto Unificado De Legislacion Secundaria Del Ministerio Del Ambiente.*, 1-40[33].

1.4.1 Nickel spectrophotometric quantification by the formation of Nickel-Dimethylglyoxime Complex

Dimethylglyoxime or $dmgH_2$, whose chemical structure is shown in **Figure 3,** is one of the most commonly used chelates in areas such as coordination chemistry and analytical chemistry; it is considered a strong field bidentate ligand[35]. In fact, the most common use of $dmgH_2$ is the formation of a square planar complex with a Ni(II) ion[36], forming a deep red solid. However, for the quantification of nickel in solution is required the formation of a soluble Ni(IV) complex with $dmgH_2$. In that case, the $[Ni(dmg)_3]^{2-}$ complex formed has an octahedral structure, in which three dmg^{2-} units are coordinated through nitrogen to the central metal[37]. They form a reddish complex when they come into contact with an alkaline nickel solution and in the presence of an oxidizing agent such as bromine. This complex has a peak of absorption approximately in 444 nm in the electromagnetic radiation spectrum, and the intensity of its color varies over time, which is why it is necessary to measure the absorbance after a fixed time, usually within 10 minutes of the formation of the complex[38].

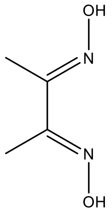

Figure 3 Dimethylglyoxime Ligand

1.5 Adsorption process for the removal of toxic metal

Adsorption is a process whereby a solid surface is exposed to a gas or liquid causing the increase in fluid density in the vicinity of an interface[39,40]. The adsorbate is the substance to be adsorbed, it is bonded in the form of a film on the surface of the adsorbent. The adsorbent is the material in which the adsorption takes place[39]. Depending on the nature of the attractive interaction force between the adsorbate molecules and the adsorbent surface, the adsorption can be classified into chemisorption and physisorption, exhibiting different behaviors and characteristics[39].

On the one hand, physisorption is referred to as reversible physical adsorption, which shows characteristics that make it more suitable for surface area determinations. It has associated low adsorption heats, and there are no violent or disruptive structural changes in the surface during adsorption measurement. Due to its reversibility, it allows studying the processes of adsorption and desorption in the same system. Physical adsorption can cover the surface by more than one layer of adsorbate and the physisorption equilibrium is achieved quickly since no activation energy is required. Molecules that have been physisorbed are not restricted to specific sites and they are free to cover the entire surface[39].

Chemisorption, meanwhile, corresponds to an irreversible adsorption process, implying a true chemical bond between the adsorbate and the surface. It shows high interaction potentials, which in turn lead to high adsorption heats. In chemisorption, the formation of a strong bond between adsorbate molecules to the surface occurs, in the presence of higher thermal energies, so that adsorption can occur. Here, the adsorbate cannot move freely across the surface due to the formation of the chemical bond between the adsorbate molecule and a specific surface site[41]. This process has related to the monolayer formation on the surface.

1.5.1 Adsorption Isotherms

An *adsorption isotherm* corresponds to the graphical representation describing the equilibrium state between adsorbate molecules and the adsorbent surface at a constant temperature. This representation generates curves that relate the equilibrium concentration of a solute on the adsorbent surface (q_e) to the concentration of the solute in the liquid (C_e) with which it is in contact. Each type of adsorption isotherm shows its respective equation of q_e as a function of C_e [39]. The more frequently of them correspond to Langmuir and Freundlich, which are detailed below.

The most important model to describe the adsorption process corresponds to *Langmuir Isotherm*, which is a semi-empirical representation derived from a proposed kinetic mechanism. This type of isotherm quantitatively describes the formation of a monolayer of adsorbate on the adsorbent surface, in which each active site interacts with a single adsorbate molecule and after that, no additional adsorption occurs on that site. An important feature of the Langmuir model is that it considers all adsorption sites energetically equivalents and there is no interaction between adjacent adsorbed molecules[39,42]. The analytical expression representing the Langmuir model is[42]:

$$q_e = \frac{Q_0 K_L C_e}{1+K_L C_e} \qquad \textbf{(1)}$$

and its linear form can be written as:

$$\frac{1}{q_e} = \frac{1}{Q_0} + \frac{1}{Q_0 K_L C_e} \tag{2}$$

The terms that appear in the previous equations corresponds to:

C_e = the equilibrium concentration of adsorbate (mg/L).

q_e = the amount of metal adsorbed per mass unit of the adsorbent at equilibrium (mg/g).

Q_0 = maximum monolayer coverage capacity (mg/g).

K_L = Equilibrium constant of the adsorption process (L/mg).

In general, most of the adsorbents of interest do not have a surface with energy homogeneity; on the contrary, they are considered energy heterogeneous solids. The representation of these adsorbents is made by the *Freundlich Isotherm*, which corresponds to a mathematical expression showing the adsorption equilibrium between the liquid (or gas) in the fluid phase with the adsorbent. This empirical model, derived in 1909, allows describing the adsorption process on heterogeneous surfaces, through which the formation of adsorbate multilayers is expected[43,44]. The equation representing this model is given by[42]:

$$q_e = K_f C_e^{\frac{1}{n}}, \tag{3}$$

whose terms q_e and C_e have the same meaning as in the Langmuir model, and the other parameters (K_f and n) correspond to:

K_f = Freundlich isotherm constant (mg/g).
n = adsorption intensity.

The linear form the Freundlich equation is:

$$log q_e = log K_f + \frac{1}{n} \log C_e. \tag{4}$$

The study of adsorption isotherms is important as it allows to determine the nature of the adsorption process, that is, to understand the interaction of the solute with the surface of the adsorbent. The resultant curve, that relates the amount of adsorbed metal in the solid and the equilibrium concentration of the metal in solution at a constant temperature can be adjusted to more than one equilibrium isotherm model[45]. Furthermore, depending on the type of isotherm, the maximum adsorption capacity of the adsorbent, as well as the amount of adsorbent required can be estimated.

CHAPTER II

EXPERIMENTAL SECTION

2.1 Materials, reagents, and equipment.

The biomass source was obtained locally, in Ecuador. The reagents and equipment used during the development of this work are specified in **Table 5** and **Table 6.** The materials used include: universal support and clamps, Soxhlet equipment, round bottom flask (150 mL), beakers (500, 200, 100, 50 mL), Büchner funnel, filter paper (4-12 µm and 1-2 µm), glass watch, spatula, glass rod, hot plate, thermometer, magnetic stirrers, plastic containers, volumetric pipette (25 mL), two neck round bottom flask, elbow, condenser, Erlenmeyer flask (250 mL), graduated pipette (1 mL), micropipettes (0.1-1 mL and 0.5-5 mL), Pasteur pipette, volumetric flask (250, 50, 10 mL), which were provided by the Yachay Tech Chemistry Laboratory.

Table 5 Reagents used in the development of this research project.

Reagents	Description	Reagents	Description
Toluene	(C_7H_8) Reactivos RD COD: 220-2	Pure Nickel Strip	SIGMA-ALDRICH 99.95%
Ethanol	(CH_3CH_2OH)	Formic Acid	(H-COOH) 98% LOBA Chemie CAS: 64-18-6
Sodium Hydroxide	(NaOH) AR® (ACS) CAS: 1310-732	Potassium Bromide	KBr SIGMA-ALDRICH ≥99% CAS: 7758-02-3
Hydrogen Peroxide	(H_2O_2) 30% Fisher Chemical CAS: 7722-84-1	Sulfuric acid	H_2SO_4 BAKER®ACS 97.99% CAS:7664-93-9
Distilled water	N.S.	Dimethylglyoxime	$C_4H_8N_2O_2$ SIGMA-ALDRICH CAS: 95-45-4
Nitric Acid	(HNO_3) 65% EMSURE® 1004562500	Ammonium Hydroxide	NH_4OH Fisher Chemical CAS: 1336-21-6
Acetic Acid (glacial)	(CH_3OH) 100% EMSURE® 1000632500	Thiourea (CH_4N_2S) 99%	LOBA Chemie CAS: 62-56-6

Table 6 Equipment used in the development of this research project

Equipment	Description
Uv-vis/NIR	Perkin Elmer / LAMBDA 1050 UV/Vis Spectrophotometer (175 to 3300 nm)
Hot plate and magnetic stirrer	MISUNG SCIENTIFIC RPM: Max. 1500 T: Max. 380 °C
Ultrasounds bath	J.P. SELECTA, s.a. 330W, 50/60 Hz
Stove	POL-EKO-APARATURA SP-J. 2500W, ~60Hz
Heating mantle	LASSCO 150W, 60
Analytical Balance	OHAUS Explorer
Thermogravimetric Analysis/ Differential Equipment	Thermal Analyzer TG/DTA SETARAM Instrumentation
FT-IR Spectrometer	Varian 670-IR
Scanning Electron Microscopy	Secondary Electron Detector JSM 6335F
NMR Spectrometer	BRUKER .AVANCE 400 Console, 9.4 Tesla magnet (400MHz)
X-Ray Difracttometer	Rigaku Miniflex 600
X-Ray Photoelectron Spectroscopy equipment	PHI 5000 Versa Probe III Scanning XPS Micropobe Ulvac phi, inc.

2.2 Cellulose extraction Methods

Cellulose was extracted from rose stems. Different treatments for cellulose extraction were developed in order to evaluate the efficiency of each of them[46]. Previous to the extraction process, the rose stems were treated as is shown in **Figure 4**; the stems were washed, cut into small pieces and dried in the oven at 50 °C until getting a constant weight. Once dried they were ground to smaller particle size and then the solid was sieved. Then, cellulose was extracted by two different treatments, one basic and one acid. The procedures for the extraction of each cellulose sample are detailed in sections 2.2.1 and 2.2.2.

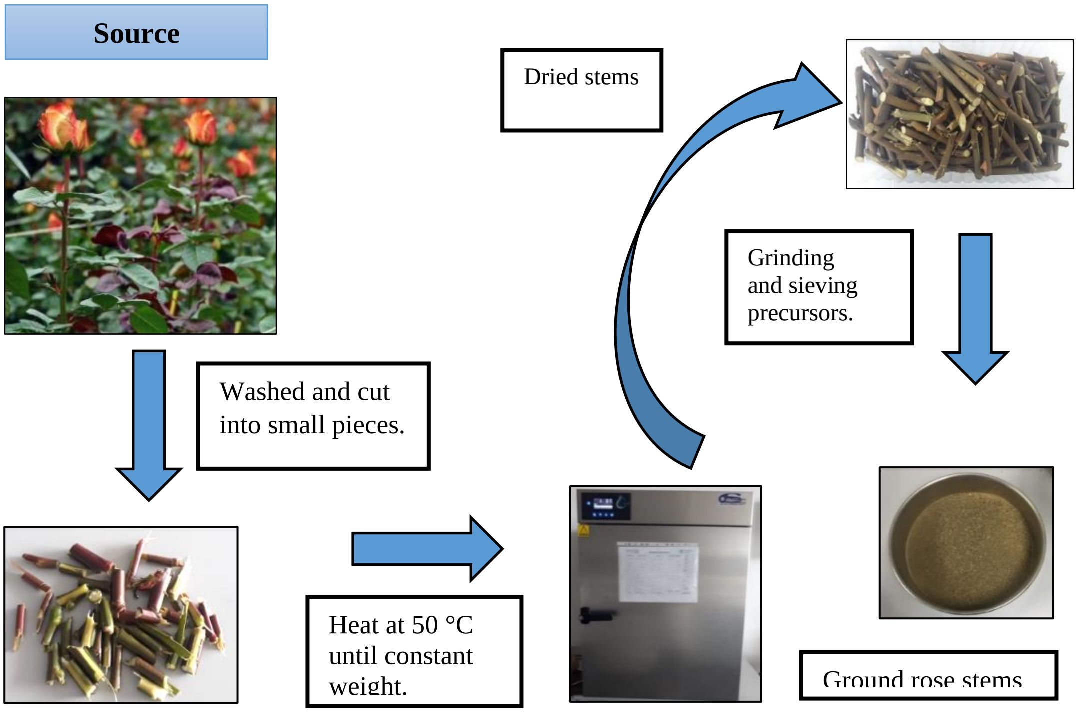

Figure 4 Process of obtaining precursors from the rose stems.

2.2.1 Alkaline extraction of cellulose from rose stems

Approximately 14 g of ground rose stems were placed in a coffee filter and carefully introduced into the Soxhlet equipment for extraction. The solvent used was toluene: ethanol mixture in a proportion 2:1. The extraction process was kept for 6 hours approximately, allowing to complete 15 cycles to ensure completeness of extraction. After that, the solid was removed from the Soxhlet equipment, washed, and it was heated in the oven at 60 °C for 16h. Then, the solid was poured in a beaker with 300 mL of distilled water and then placed in an ultrasound bath at 55 °C for 40 minutes. After that, it was filtered, and the resulting solid was mixed with 200 mL of 0.5 M NaOH and 3% H_2O_2, and then was added 200 mL of 2 M NaOH. Finally, the mixture was heated at 55 °C for 2h in a hot plate, then, it was cooled to room temperature, filtered, washed, and the resulting material dried in an oven at 60 °C for the subsequent recording of its weight. The solid obtained by this procedure was labeled as CRT.

2.2.2 Acid extraction of cellulose from rose stems

A mixture of acetic acid: nitric acid in a ratio 10:1 was poured in a beaker containing ~5 g of ground rose stems and mixed with the help of a glass rod. Then, the beaker containing the mixture was placed in a sand bath to be heated to 110-120 °C for 20 minutes. After heating, the mixture was allowed to reach room temperature, and then 60 mL of distilled water was added. The mixture was separated by filtration, washing the solid with abundant ethanol and water until the filtrate reached a neutral pH. Finally, the solid was dried at 60 °C for the subsequent recording of its weight. The solid obtained by this procedure was labeled as CRA_2.

2.3 Modification of CRA_2 sample

To evaluate a potential improvement in its adsorption capacity, the cellulose was modified using thiourea. The sample that was treated with thiourea was only CRA_2, this was chosen due to the lower environmental impact generated by its extraction process and its replicability. The modification process was as follows: 1g of cellulose extracted was mixed with 20 mL of a 0.5 M solution of thiourea (in ethanol); the mixture was allowed to be in contact for 24 h. Then, the solid was filtered and washed with distilled water; and finally, the solid was dried in an oven at 50 °C for 24 h. Chemically modified cellulose sample was labeled with the letter F after their initial code (CRA_2F).

2.4 Spectrophotometric Determination of Nickel (II)

In the following subsections, the spectrophotometric methods implemented in this research are detailed.

2.4.1 Preparation of stock and sub-stock solutions

To obtain the stock solution of Ni(II) 0.8020 g of nickel 99.95% was weighed on a 0.1 mg precision balance and dissolved in 15 mL of HNO_3 65% at 80 °C for 1h. Once the nickel was dissolved, the resulting solution was transferred to a 250 mL volumetric flask and flush with distilled water to prepare the stock solution with a concentration of 3195.22 mg/L (ppm). From this stock solution, 7.8 mL were taken to prepare a 50 mL sub-stock solution (498.5 ppm). Both solutions were properly stored for later use.

2.4.2 Preparation of standards solutions

Standards solutions of $[Ni(dmg)_3]^{2-}$ complex (ranging from 1 to 10 ppm) were obtained through the oxidation of Ni(II) to Ni(IV) using a saturated solution of bromine water as the oxidizing agent and the subsequent treatment of the Ni(IV) ions in an ammonia solution with $dmgH_2$ was followed.

The procedure, represented in **Figure 5**, was as follows:

- Aliquots of sub-stock solution were poured in 50 mL volumetric flasks following the specifications in **Table 7**, in order to obtain each desired NI(II) concentration.
- 1 mL of bromine water was added directly to each of the flasks and set to rest for ~3min (after which time it is assumed that the oxidation reaction, Ni(II) to Ni(IV), took place).
- A basic medium for complex formation was required, for which 2 mL of concentrated NH_4OH were added to each of the flasks.
- Once the appropriate pH condition was achieved, 1 mL of 1% DMG was added in each of the flasks. At this point, the solution, initially turquoise blue, turned red indicating the presence of $[Ni(dmg)_3]^{2-}$ complex.
- Finally, each solution was diluted with distillate water obtaining Ni(IV) solutions at different concentrations, showing variation in the red intensity from slight (the most diluted) to intense red (the most concentrated). The nickel concentration was measured by UV-Vis spectroscopy, measuring the absorption of $[Ni(dmg)_3]^{2-}$ complex.

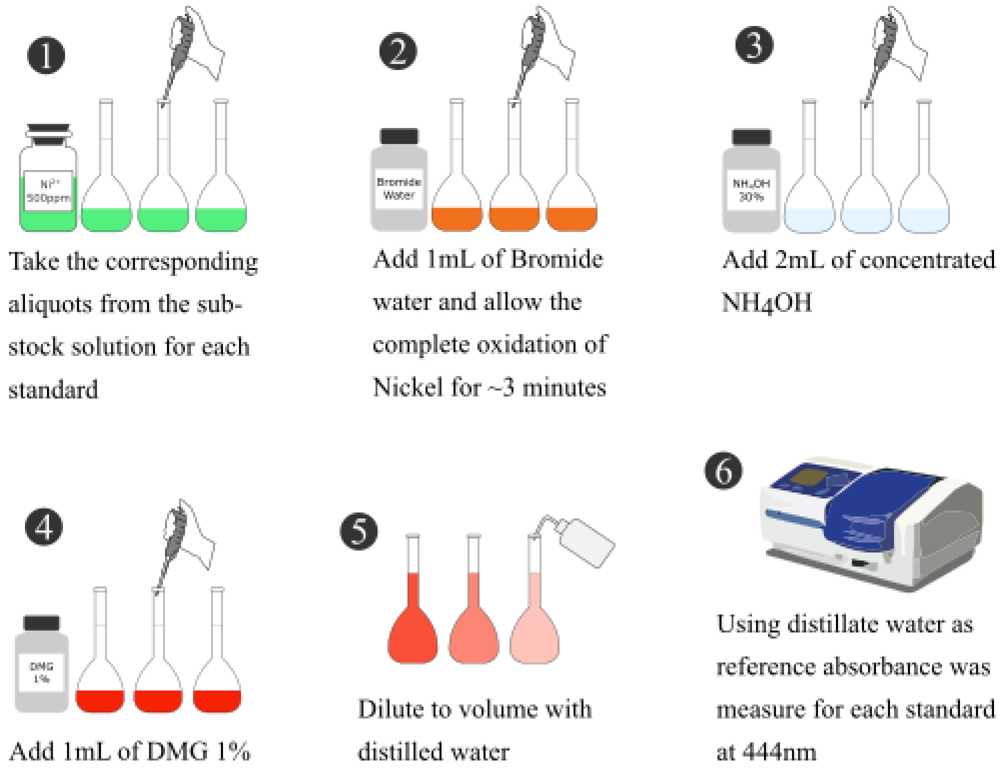

Take the corresponding aliquots from the sub-stock solution for each standard

Add 1mL of Bromide water and allow the complete oxidation of Nickel for ~3 minutes

Add 2mL of concentrated NH_4OH

Add 1mL of DMG 1%

Dilute to volume with distilled water

Using distillate water as reference absorbance was measure for each standard at 444nm

Figure 5 Schematic representation of $[Ni(dmg)_3]^2$ complex formation.

Table 7 Aliquot needed to prepare 50 mL of standard solutions with a concentration between 1-10 ppm.

Standard solution (ppm) (±0.1)	Aliquot from sub-stock solution Ni(II) (mL) (±0.15% precision)
1.0	100
2.0	200
3.0	300
4.0	400
5.0	500
6.0	600
7.0	700
8.0	800
9.0	900
10.0	1000

Bromine water preparation

Initially, 25 g of KBr were weighed and poured in a two neck round bottom flask, connecting in one of the necks a separating funnel containing ~50 mL of H_2SO_4 conc. and in another one, an elbow connected to a condenser through which bromine vapors condensed. The schematic representation of the experimental set-up is shown in **Figure 6.** The round bottom flask was placed on a hot plate at 60 °C and proceeded to the slow addition of the acid. Once all the acid was added, 25 mL of 30% H_2O_2 was poured into the separating funnel with the objective of making the reaction of bromine formation more quickly. Finally, condensed vapors were collected, drop by drop, in a flask containing a little amount of distilled water, arranged at the end of the condenser and introduced into a water/ice bath.

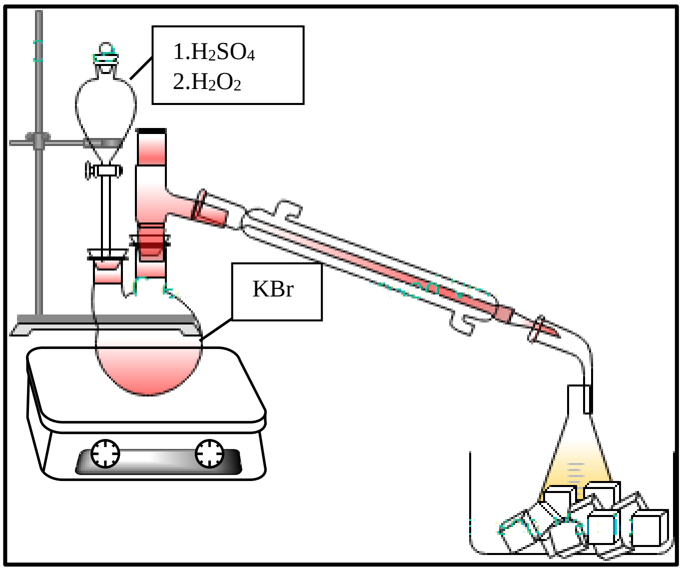

Figure 6 Schematic representation of Bromine water obtaining.

Source: Designed from ChemDraw and EdrawMax Software.

Dimethylglyoxime 1% Preparation

A 1% dimethylglyoxime ($dmgH_2$) solution was prepared by dissolving 1.0402 g of this compound in 100 mL of mixture methanol: distilled H_2O 30:70. To help with the dissolution of $dmgH_2$, the flask was placed on a stirrer plate during a few minutes.

2.4.3 Calibration curve and measurements of concentrations of nickel

From the standards solutions obtained through the process described in section 2.4.2, a calibration curve was constructed. The UV-Vis absorption of the complex $[Ni(dmg)_3]^{2-}$ in each sample was recorded at 444 nm. The determination of nickel concentration for all of the samples was made by using a double beam UV/Vis Spectrophotometer, using distillate water as a reference, and within 10 minutes of the formation of the complex.

2.5 Adsorption process of Ni(II) on cellulose samples

Initially, 4 mL of the stock solution was placed in a 250 mL volumetric flask, flushing with distilled water, to reach a Ni(II) solution with a concentration of 51.12 mg/L. For adsorption experiments, the initial concentration of nickel solution was kept constant at this value, and the amount of cellulose-based adsorbent was changed. The different amounts of adsorbent tested were: 5, 10, 15, 25, 50, 75, 100, 125, 150 and 350 mg, which were placed in different beakers previously labeled. Into each of them, 25 mL of 51.12 mg/L Ni(II) solution were added, which were subjected to stirring, using a stir plate for

48h and at a speed of 250 rpm. After that, the mixture was filtered and both solid (adsorbent) and solution were stored for further analysis. The nickel species quantification in solution was carried out following the same procedure for the standard solutions described in section 2.4.2. In this case, aliquots of 1 mL were used to reach a final volume of 10 mL.

2.6 Characterization techniques for the analysis of nickel solutions and adsorbents samples.

Ultraviolet-Visible (UV-Vis) Spectroscopy

UV-Vis spectroscopy is a quantitative analytical technique, which studies the absorption of radiation by chemical species in the near-infrared-ultraviolet zone (180–390 nm) and the visible range (390–780 nm) of the electromagnetic spectrum. As a result of energy absorption, atoms or molecules move from a fundamental state to an excited state. The lowest-energy occupied molecular orbitals are the σ and π orbitals, and the orbitals of the highest energy are antibonding orbitals (σ* and π*). In addition, the relationship between absorbance and the concentration of the analyte in solution is known as the Lambert-Beer law:

$$A=\varepsilon l C\ , \qquad \mathbf{(5)}$$

where A is the absorbance of the solution (without units); ε is the molar absorption capacity (L mol^{-1} cm^{-1}), l is the length of the radiation path through the absorbent medium (cm); and C is the concentration (mol L^{-1}) [47,48]. The absorbances of the solutions were measured using a double beam UV/Vis spectrophotometer at a wavelength of 444 nm.

Fourier Transform Infrared Spectroscopy (FT-IR)

Fourier Transform Infrared Spectroscopy is used in the characterization of different compounds to identify the functional groups present in the samples. Infrared radiation, which corresponds to energy changes on the order of 8 to 40 kJ/mole, is absorbed by molecules when they are excited to a higher state of energy. Within this range, the stretching and bending vibrational frequencies of the bonds in the molecules are found[48]. FTIR measurements of cellulose samples were taken using Varian 670-IR Spectrometer, with 32 scans in the range from 400 to 4000 cm^{-1} and a resolution of 4 cm^{-1}. The samples were finely ground using a mortar and mixed with potassium bromide (KBr), the mixture was compressed as a pastille.

Nuclear Magnetic Resonance (NMR)

Nuclear Magnetic Resonance is a technique used mainly in the elucidation of chemical structures. ^{13}C NMR allows the identification of carbon atoms in different chemical environments[48]. In this research, the NMR spectra were taken on a BRUKER NMR Spectrometer 400 MHz using Cross Polarization Magic Angle Spinning CP-MAS and High Power ^{1}H Decoupling.

CP-MAS experiment involves transferring the polarization of abundant nuclei such as ^{1}H or ^{19}F to isotopically scarce nuclei such as ^{13}C, ^{15}N or ^{29}Si, helping to increase the sensitivity of the experiment. The magnetization transfer requires that the non-sensitive nucleus be dipolar coupled with the proton nuclei. Furthermore, CP takes place while the sample spins rapidly around the magic angle, for this reason, it is called Cross Polarization Magic Angle Spinning[48,49]. And High Power ^{1}H Decoupling experiment the sample is also spins rapidly around the magic angle averaging of the dipolar couplings ^{13}C - ^{1}H[50].

X-ray Photoelectron Spectroscopy (XPS)

X-ray Photoelectron Spectroscopy (XPS) is a useful technique for analysis of the composition of a material, both qualitative and quantitative. Also, it provides information on the chemical state of the elements on the surface of a material[51]. Electron spectroscopy techniques measure the kinetic energy of electrons emitted by matter because it is bombarded with ionizing radiation or high energy particles[52]. XPS equipment was used (PHI 5000 Probe III Scanning XPS Micropobe, Ulvac phi,inc) in order to obtain the results.

X-ray Diffraction (XRD)

X-ray Diffraction (XRD) is an analytical technique used primarily for the identification and quantification of crystalline and amorphous phases present in a material providing information about its structure[53]. In addition, each crystalline solid has its own characteristic XRD pattern that can be used as a "fingerprint" for its identification[52]. X-rays are electromagnetic radiation of wavelength ~1 Å (10^{-10} m). The most common method used to determine the crystallinity index (CrI) is the proposed by Segal[54], this method only explain the relative differences of CrI between samples, **Eq. 6** is used to calculate it. In this equation, I_{002} is the height of the (002) peak and I_{AM} is the lowest height between the (002) and (101) peaks, as you can see in **Figure 7**.

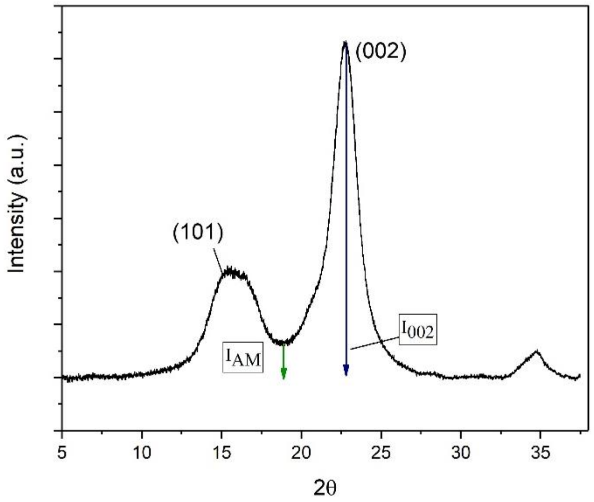

$$CI\ \% = \frac{I_{002} - I_{AM}}{I_{002}} \qquad \textbf{(6)}$$

Figure 7 Diffraction pattern showing the difference of the intensities of the associated peaks to (002) and (101) planes for cellulose (left). Equation suggested by Segal and coworkers to calculate CrI% (right).

The samples were analyzed using a Rigaku Miniflex 600 X-ray diffractometer with a monochromatic CuKα radiation source (λ= 0.1539 nm), 40 kV and 20 mA in a range from 10° to 40° with a scanning time of 25 min.

Scanning Electron Microscopy (SEM)

Scanning Electron Microscopy (SEM) is a technique that allows obtaining high-resolution imaging of a material surface. In SEM an electron beam is generated, which is focused by a series of electromagnetic lenses. Due to the interaction of the beam with the sample a signal is generated that is collected and processed to generate an image[55]. Qualitative and quantitative chemical analysis information is also obtained using an Energy Dispersive X-ray Spectroscopy (EDS) technique coupled with the SEM[56]. This technique allows to detect the x-rays emitted from the sample during bombardment by the electron beam[57]. Micrographs were obtained using a JSM 6335F Scanning Electron Microscope operated in secondary electron mode, and an accelerating voltage of 15 kV. Samples were previously coated with gold for 50 seconds using a Q150RS QUORUM-Rotary Pumped Coater. Images were obtained with magnifications of 200X and 1000X.

Thermogravimetric Analysis (TGA)

Thermogravimetric Analysis gives complementary useful information. On the one hand, TGA is a technique used to evaluate the thermal stability of a material, in which the mass of a sample is measured as a function of temperature over time[58]. In addition, derivative thermogravimetry (DTG) corresponds to the first derivative of the TGA curve and helps to a better interpretation of the data by determining the inflection points present. Thermogravimetry/derivative thermogravimetry (TG/DTG) and Differential Thermal Analysis are used to investigate the thermal behavior of CRA_2 and CRA_2F samples. The DTA thermograms were obtained using a Differential Thermal Analyzer at a 10 °C/min heating rate, from 20 °C to 600 °C. Helium gas was used as an inert medium during the thermal analysis, the amount of material used was 11 mg and the reference material was aluminum oxide.

Textural Characterization

The textural properties of a solid such as specific surface area, volume and pore size are determined using a technique based on gas adsorption. The results of the analysis show an adsorption-desorption isotherm, where the data obtained are related to the volume of gas retained by the surface of the sample under certain pressure conditions. The mostly used gas is nitrogen at 77 K and the standard method for determining the previously defined parameters is related to the representation of Brunauer-Emmett-Teller (BET) isotherm from the data obtained. Once the number of gas molecules necessary to form a monolayer is obtained by BET, and knowing the area occupied by one of these adsorbed molecules it is possible to estimate the specific surface area of the solid. Specific surface area is defined as the total surface area of a material per unit of mass (m^2/g), while total pore volume refers to the volume occupied by adsorbate within the adsorbent (cm^3/g)[59,60]. The textural analysis of CRA_2 and CRA_2F was performed using a Micromeritics ASAP 2010 by nitrogen adsorption at 77 K.

CHAPTER III

RESULTS, INTERPRETATION, AND DISCUSSION

3.1.Cellulose Samples

Two cellulose samples were extracted applying different treatments to the precursor and CRA_2 was further treated with thiourea. The scheme shown in **Figure 8** is a summary of the samples prepared (CRT, CRA_2, and CRA_2F), and the one used as standard (CS) obtained from Sigma Aldrich. In order to give more reliable results, each experiment was repeated three times under the same conditions and the yield of the extraction was given as the average of the experiments. These yields are specified in **Table 8**, which were calculated using the **Eq. 7**.

$$\%yield = \frac{actual\ yield}{theoretical\ yield} x100\ \% \tag{7}$$

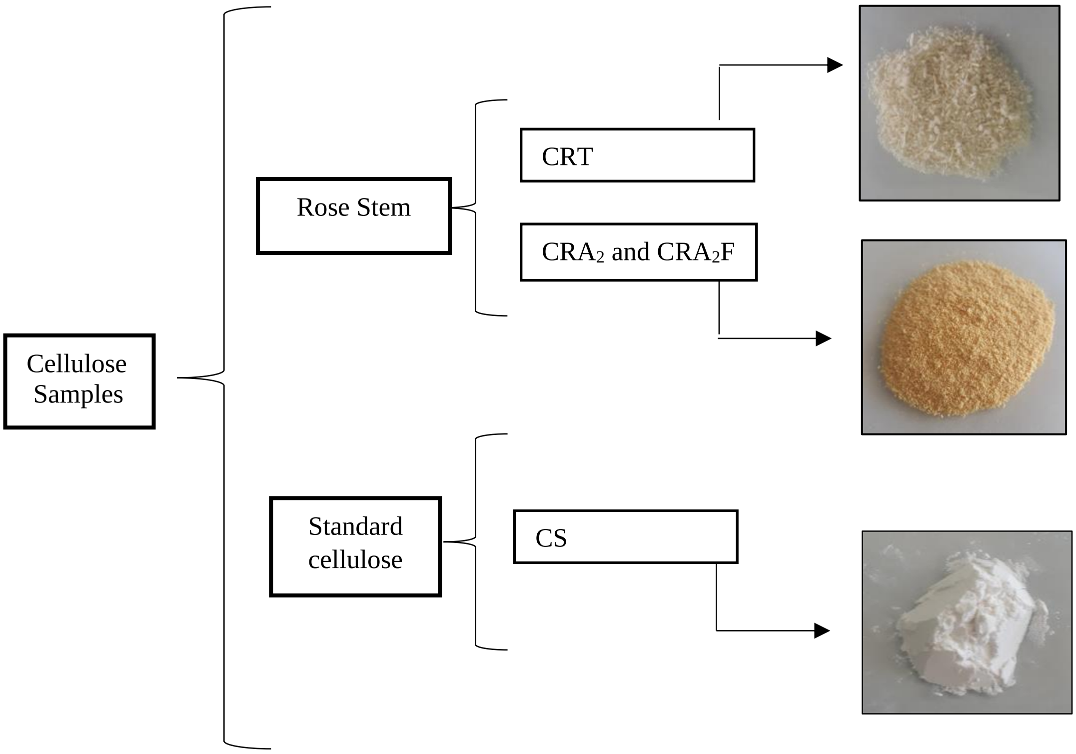

Figure 8 Scheme that summarizes the samples used in this research project.

The results obtained in **Table 8** show that the CRA_2 sample has a higher percentage than expected according to data reported. This difference may be due to the fact that the obtained samples were not completely pure, suggesting the presence of lignin and hemicelluloses still attached even to the surface of cellulose fiber. These doubts will be clarified later in the analysis of the characterization techniques.

Table 8 Average of the yield of each of the samples obtained.

Samples	Treatment	Yield (%)	Reported %Cellulose present in rose steam
CRT	Alkaline	47.20%	45-50
CRA$_2$	Acid	59.92%	

3.1.1. CRT Sample preparation

Initially, the biomass source was treated with the mixture toluene: ethanol in a 2:1 ratio, to eliminate pigments, waxes, and oils present in the initial sample. The use of sonication and alkaline treatment together with the addition of 3% hydrogen peroxide helped in the degradation of hemicelluloses and lignin present in the rose stem. In this case, H_2O_2 reacted with lignin under alkaline conditions, contributing to the delignification and bleaching process. It is assumed that hydrogen peroxide has the capacity to react with various carbonyl-containing structures in lignin through the hydroperoxide anion (HOO^-) formed in an alkaline medium ($H_2O_2+HO^- \leftrightarrow HOO^-+H_2O$), this being a strong nucleophile that attacks carbonyl groups present in lignin, removing chromophores during the bleaching process[46,61].

3.1.2. CRA$_2$ Sample Preparation

Through this method, cellulose was isolated by a single step, unlike the previous methods of extraction. The acid mixture used in this case contributed to the delignification process as well as the elimination of non-cellulosic polysaccharides. The treatment with 80% acetic acid using 70% nitric acid as an extraction solvent is considered a good method based on organic acid to isolate cellulose fraction[62]. This process is free of chlorinated compounds usually used for bleaching and delignification process[46,63].

3.2. Solid characterization

3.2.1. Fourier-transform infrared spectroscopy (FT-IR)

In **Figure 9**, the FT-IR spectrum of the precursor (rose stems) used for cellulose extraction is shown, in which is observed the presence of peaks corresponding to lignocellulosic biomass[64]. Not all peaks in the spectrum of the precursor correspond to cellulose structure, but also to other species, such as lignin and hemicellulose, present in the biomass. These peaks are located at:

1735 cm^{-1} ⇒ C=O stretching of the acetyl groups present in hemicellulose and lignin structures[64].

1640 cm^{-1} ⇒ Bending mode of the adsorbed water[64].

1508 cm^{-1} ⇒ C=C stretching present in the aromatic skeleton of lignin[19].

1260 cm^{-1} ⇒ Stretching of C-O in hemicellulose structure[65],

801 cm^{-1} ⇒ C-H deformation out of plane corresponding to aromatic ring [66,67].

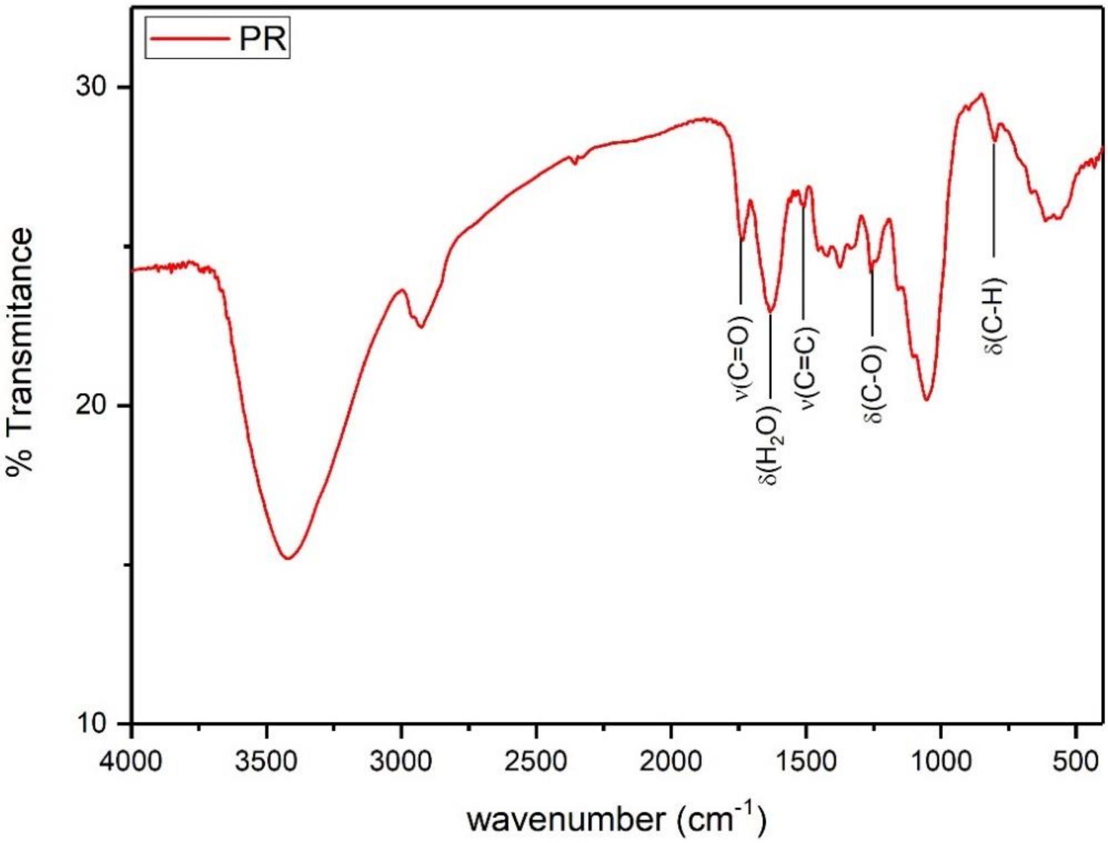

Figure 9 FT- IR spectrum of PR (rose stems) precursor.

Figure 10 shows a comparison of the FT-IR spectra of CS, CRA_2, and CRT samples. The spectra of CRA_2 and CRT show similar peaks to the spectrum of the standard cellulose (CS). For example, the peak at 3401 cm^{-1} due to the stretching of O-H groups, the one at 2902 cm^{-1} attributed to C-H stretching in CH_2 and CH_3 groups[46]. In addition, the peak at

1430 cm^{-1} indicates the bending mode of CH_2 groups and the one located at 1372 cm^{-1} is associated with O-H bending. The peak at 1162 cm^{-1} is due to antisymmetric bridge stretching, the peak corresponding to the C-O-C pyranose ring skeletal vibration can be appreciated in the region 1076-1023 cm^{-1} and the peak at 897 cm^{-1} is due to the β-glycosidic bond between glucose units in cellulose[46,62].

In contrast to the CS and CRT spectra, the CRA_2 sample shows a peak at 1735 cm^{-1} corresponding to the C=O vibration, which is more intense than the one observed in the precursors. This could be related to the treatment of biomass under acidic conditions to which the biomass was subjected. However, the value of 1735 cm^{-1} is characteristic of a carbonyl in the ester group, and not in an acidic one[48]. Moreover, it was observed that in CRT and CRA_2 samples there was still a presence of lignin and hemicellulose, which is evidenced by the peaks shown at 1505 cm^{-1} and 1256 cm^{-1}, although not with the same intensity in the precursor spectrum.

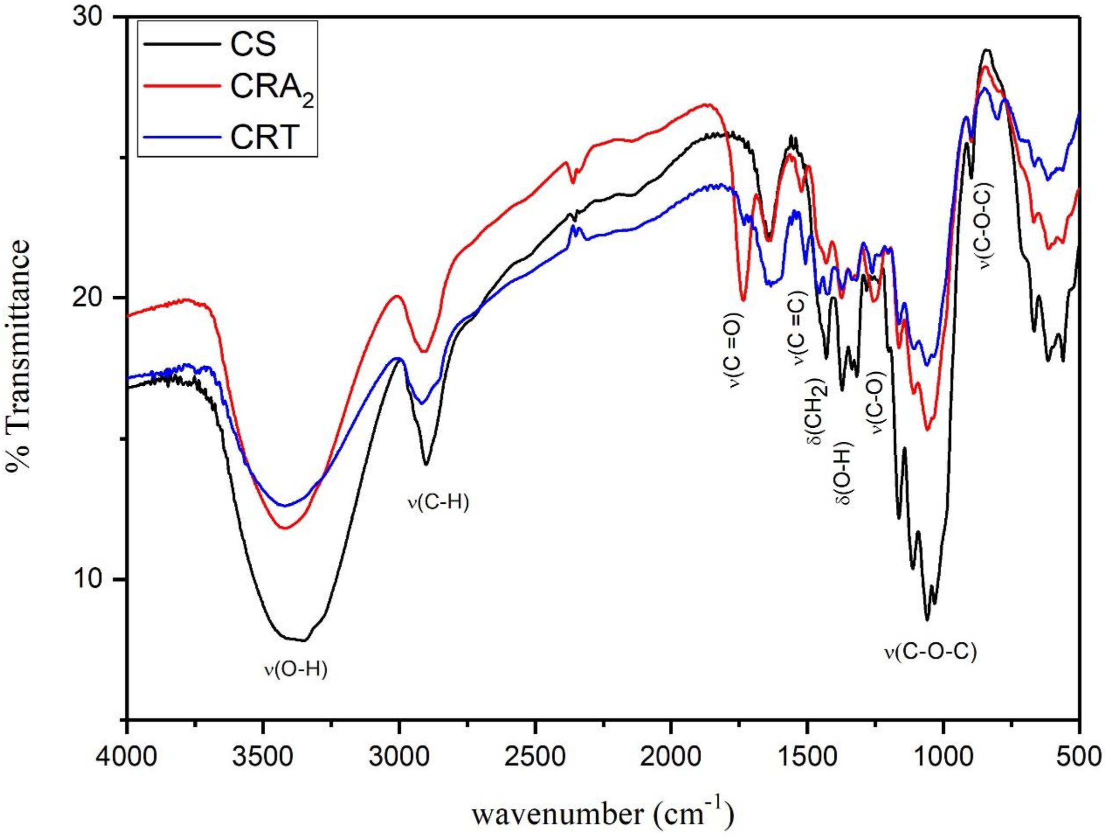

Figure 10 FT-IR spectra comparison of cellulose standard (CS), CRA_2, CRT

The sample chosen for subsequent chemical modification was CRA_2, it was treated with thiourea in order to modify the cellulose structure, obtaining a sample that was denoted by CRA_2F. The spectrum of thiourea is shown in **Figure 11**. This compound shows two near peaks at 3368 cm^{-1} and 3263 cm^{-1} due to the antisymmetric stretching of NH_2, the peak at 2685 cm^{-1} is attributed to symmetric steching of NH_2 group. An intense peak is observed at 1603 cm^{-1} associated with the bending mode of NH_2. The antisymmetric and symmetric stretching of CN appears at 1462 cm^{-1} and 1081 cm^{-1}, respectively. Finally, the antisymmetric stretching of C=S is located at 1406 cm^{-1} and the symmetric stretching at 728 cm^{-1} [5,68].

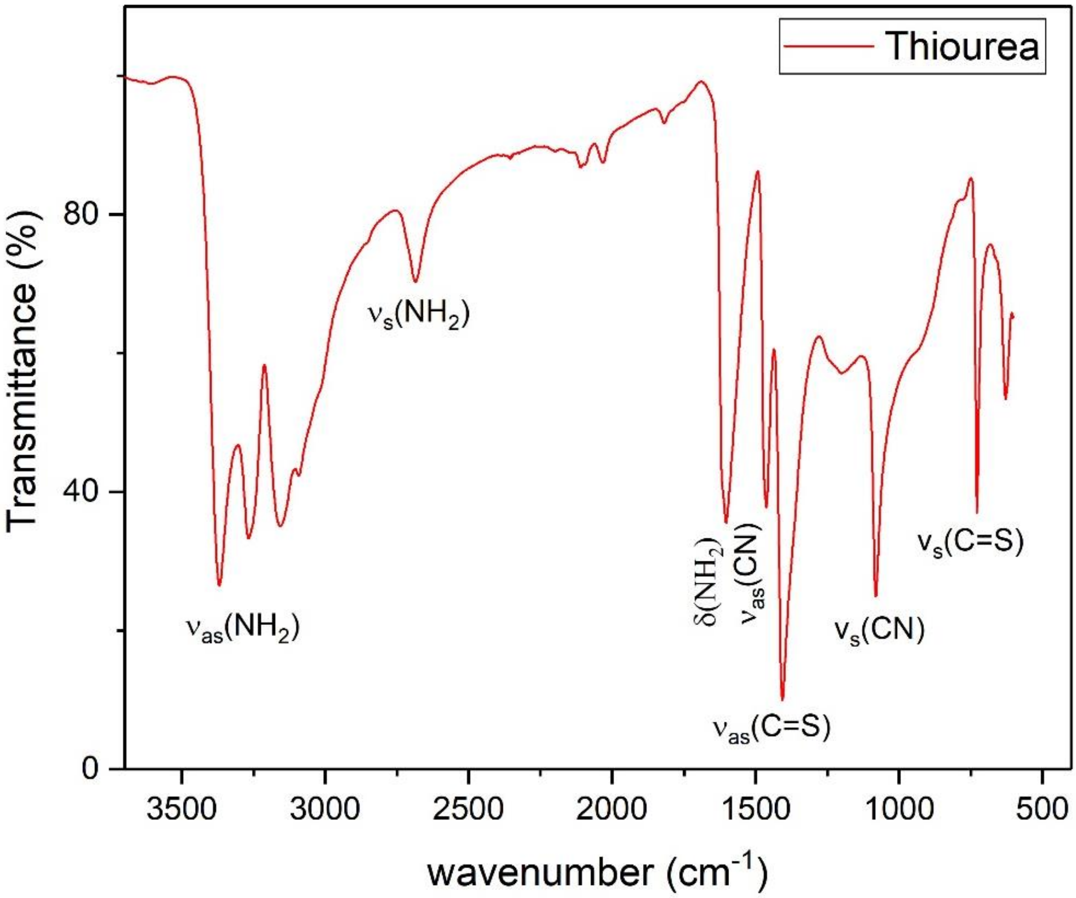

Figure 11 FI-IR spectrum of thiourea.

In **Figure 12** it is shown a compilation of the FTIR spectra of the unmodified (CRA_2) and modified cellulose (CRA_2F) using thiourea. The appearance of the peaks at 1624 cm^{-1}, 1418 cm-^{1}, 1395 $cm^{-1,}$ and 729 cm^{-1} suggests the presence of thiourea in the sample. The signal at 1624 cm^{-1} is attributed to the bending vibration of the NH_2 group, the asymmetric stretching of the CN appears approximately at 1418 cm^{-1}, and the antisymmetric and symmetric vibration of the C=S appear at 1396 cm^{-1} and 729 cm^{-1}, respectively.

The values of the peaks presented in the spectrum of CRA$_2$F differ from those shown by thiourea in **Figure 11** and in the literature[5,68]. These small displacements in the position of the peaks may be associated with the interaction of thiourea and cellulose due to chemical modification achieved. However, to ensure the incorporation of thiourea in the structure of cellulose, other techniques were developed, which are detailed below. Other signals attribute to this incorporation cannot be observed due to the more intense peaks that cellulose presented in those regions.

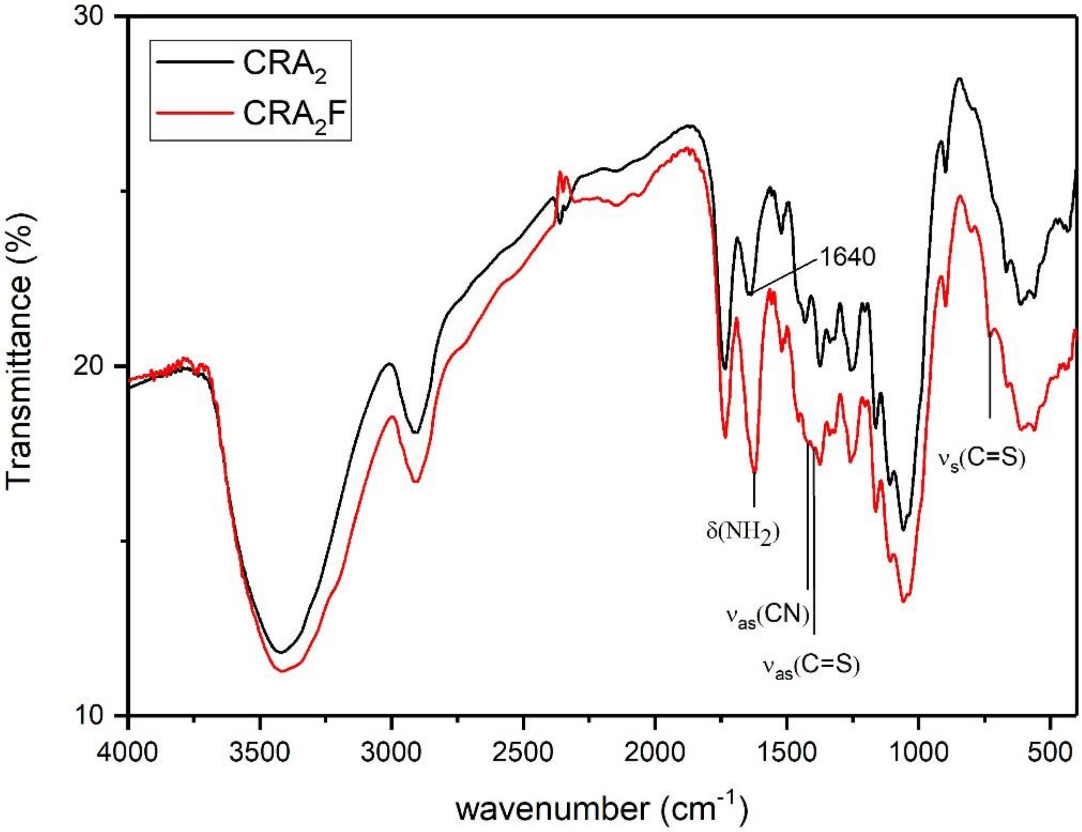

Figure 12 FT-IR Spectra comparison of CRA$_2$ and CRA$_2$F.

3.2.2 Scanning Electron Microscopy -Energy Dispersive X-Ray Spectroscopy (SEM-EDS)

Figure 13-A and **Figure 14-A** show the SEM images at different magnifications of fibrils of cellulose corresponding to CRA$_2$ and CRA$_2$F samples. The intermolecular hydrogen bonds represent the main factor that holds together cellulose chains forming the fibrous structure that can be observed[69]. Furthermore, there is also the presence of particles with

different sizes and not regular shapes, this can be attributed to the presence of lignin and hemicellulose that still persists in the fibers[70], previously confirmed by FT-IR spectra. In micrographs can be appreciated small holes in the cellulose fibers, which give the appearance of being pores, this could be attributed to the acid treatment used to try to remove hemicelluloses and lignin. However, the contribution of these pores to the adsorption capacity of obtained material was not relevant, due to their very little size, as will be confirmed with further analysis.

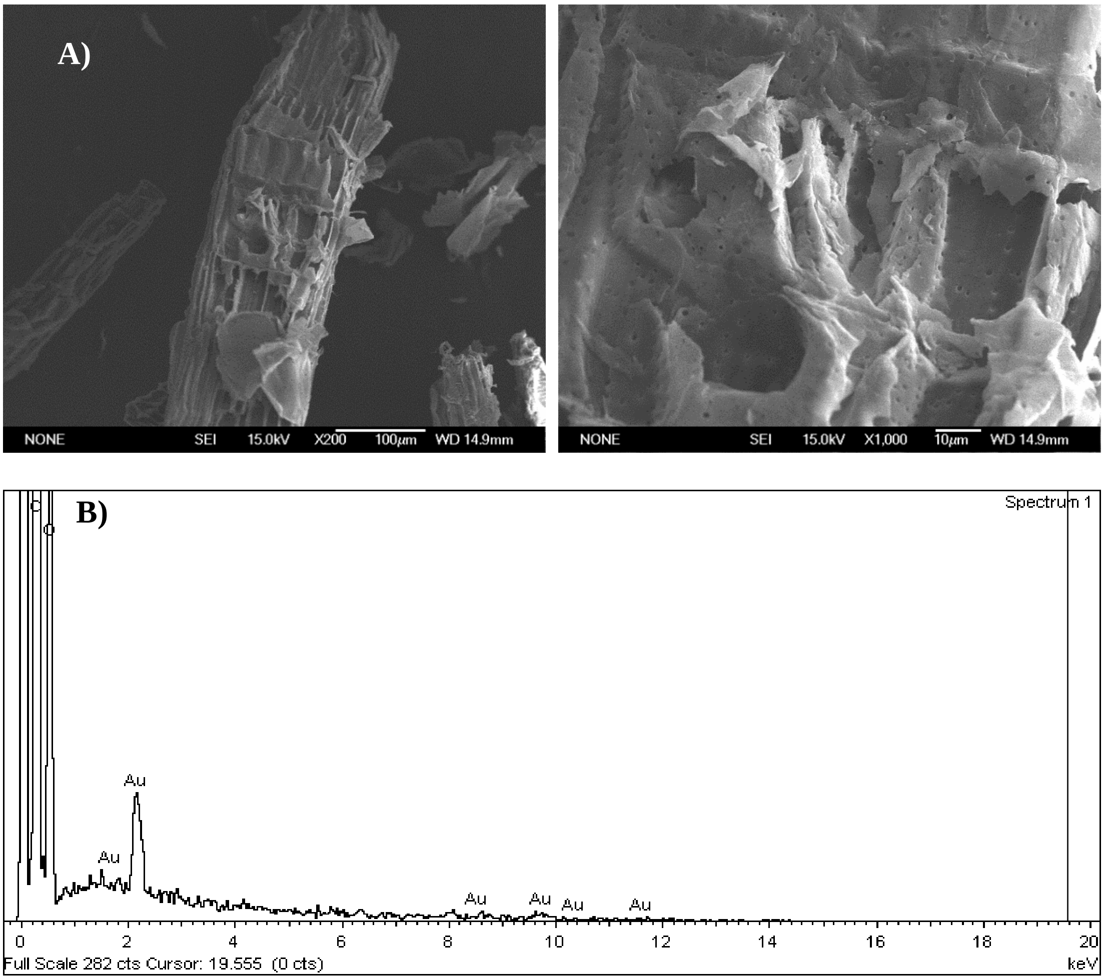

Figure 13 A) SEM images of CRA$_2$ under different magnification, 200x and 1000x. **B)** EDX spectrum of CRA$_2$.

In addition, EDS analyses showing the surface composition of the obtained material are presented in **Figure 13-B** and **Figure 14-B**. On the one hand, as expected, in all samples it was observed the presence of elements such as carbon and oxygen due to the structure itself of lignocellulosic compounds. Moreover, the EDS spectrum of CRA$_2$F shows the presence of sulfur due to the use of thiourea in the modification process.

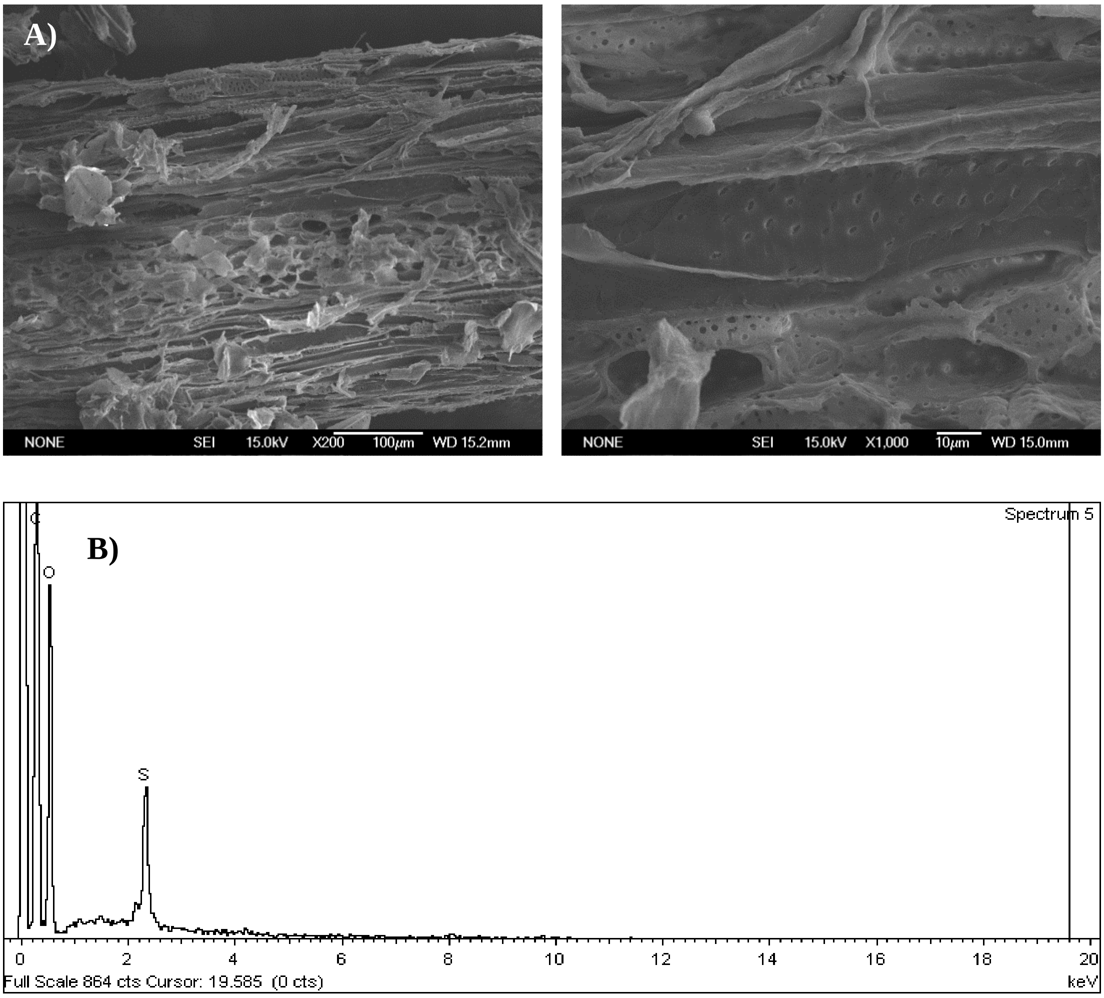

Figure 14 A) SEM images of CRA_2F under different magnification (a) 200x (b) 1000x. **B)** EDX spectrum of CRA_2F.

3.2.3 Textural Characterization

Total specific surface area (S_{BET}), pore-volume (V_T), and pore diameter (D_p) of CRA_2 and CRA_2F samples were determined by the BET isotherm through the surface analysis carried out. In **Table 9**, the values obtained for these characteristics are indicated. The results show cellulose fibers with very small specific surface area values and small pore diameter values ranged 15-17 Å, so the samples can be considered not porous. According to the literature, S_{BET} values for cellulose fibers are small, even lower than those reported in this work[71,72]. In addition, and in accordance with some reported results, a decrease in S_{BET} of the modified sample was observed, which can be due to the presence of thiourea occupying part of cellulose surface[5].

Table 9 Results of the textural characterization of cellulose samples

Sample	S_{BET} (m^2g^{-1})	V_T (cm^3g^{-1})	D_p (Å)
CRA_2	1.8346	0.003592	15.8974
CRA_2F	1.6874	0.002081	17.3177

3.2.4 Cross Polarization-Magic Angle Spinning (CP-MAS) Nuclear Magnetic Resonance ^{13}C Spectra

In **Figure 15** CP/MAS ^{13}C NMR spectra of CRA_2 and CRA_2F are shown. The two peaks at 62.56 and 64.89 ppm are assigned to carbon six (C6) of cellulose, in which 62.56 represents the amorphous part and 64.8 ppm the crystalline one[46,73]. The group of resonances from 72.09 to 74.74 ppm is attributed to C-2, C-3, and C-5. Then, the next two peaks at 83.54 and 88.74 ppm are due to C-4, in which 88.74 ppm represents the crystalline part of cellulose, and 83.54 ppm the amorphous part[63,70]. The peak at 104.89 ppm is attributed to C-1 of cellulose, this appears mostly displaced with respect to the other carbons of cellulose backbone due to its proximity to the oxygens of the structure[46,70]. The signals at 171.93 ppm (C-7) and 21.13 ppm (C-8) corroborates the information provided by FT-IR, which shows that cellulose sample has been acetylated in the extraction process due to the use of acidic mixture[74].

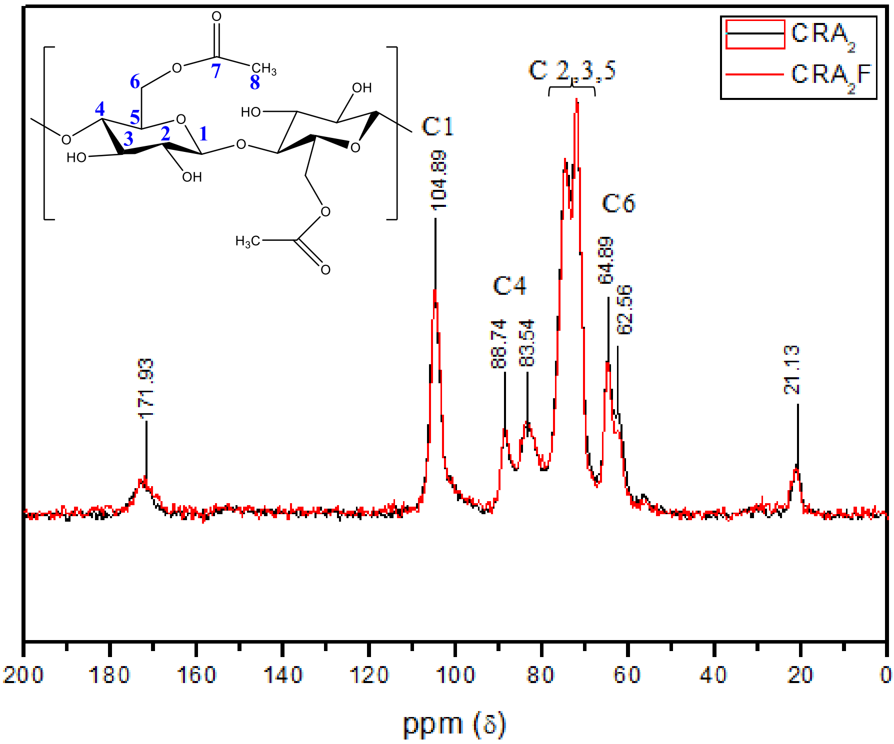

Figure 15 ^{13}C CP-MAS NMR spectrum comparison between CRA_2 and CRA_2F.

In order to visualize the peak corresponding to the thiourea carbon, the method of *High-Power Decoupling* was used. As can see in **Figure 16**, there is a small and wide peak centered in 182 ppm which would correspond to the signal of carbon in the thiourea structure. According to the literature, ^{13}C NMR of thiourea shows a triplet at approximately 183.7 ppm due to the coupling of the two equivalent N atoms[75]. So, with this small difference in both signals, it is not possible to affirm or discard the linkage of the thiourea to the cellulose structure.

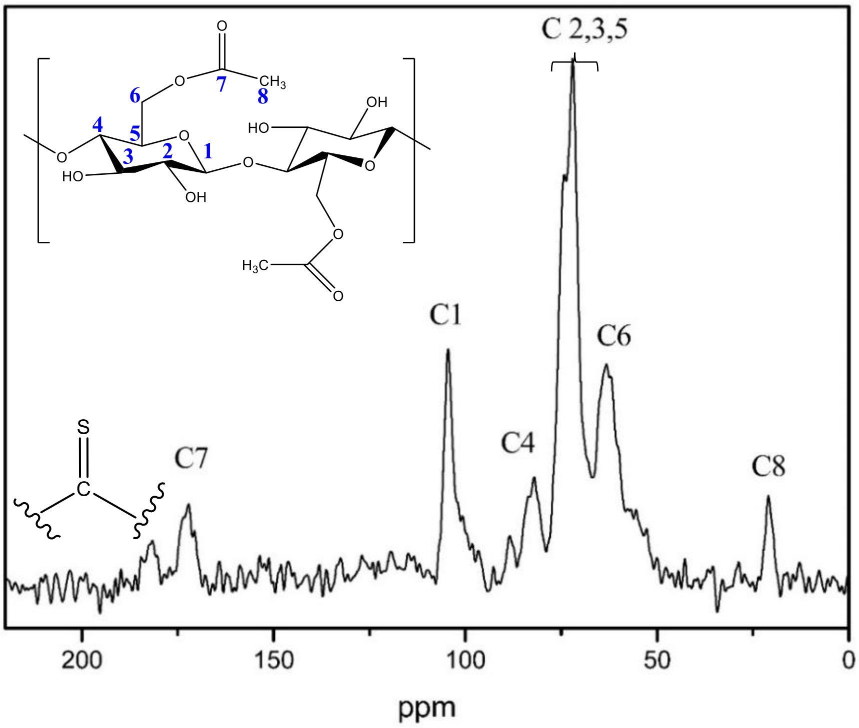

Figure 16 ^{13}C NMR with High Power Decoupling of CRA$_2$F sample.

3.2.5 TGA Analysis

Due to their chemical structures, cellulose, hemicellulose, and lignin have different thermal stability, and therefore their decomposition temperatures are different. To evaluate the thermal stability of CRA$_2$ and CRA$_2$F samples in which the presence of lignin and hemicellulose has already been verified, thermogravimetric analysis was carried out. The respective thermograms of the samples are shown in **Figure 17**. As can be seen in the DTG curve of CRA$_2$, three different peaks are present, the first one occurring in a temperature range of 50-120 °C, which corresponds to the release of absorbed water by natural fibers and decomposition of very light volatile compounds[76,77]. The second stage of degradation, which is due to the breakdown of hemicellulose is reported to appear in a range of 220-300 °C[78], and for the sample under study in this work, the decomposition peak reached the maximum at 257 °C. Finally, according to literature, the main stage of degradation corresponds to the depolymerization of cellulose, it usually occurs in the range of 315 – 400 °C with a maximum peak at 331°C[79]. For the case of CRA_2 sample, the maximum peak was reached at 321 °C. This difference in the maximum degradation temperature could be associated with differences in the crystallinity in both samples.

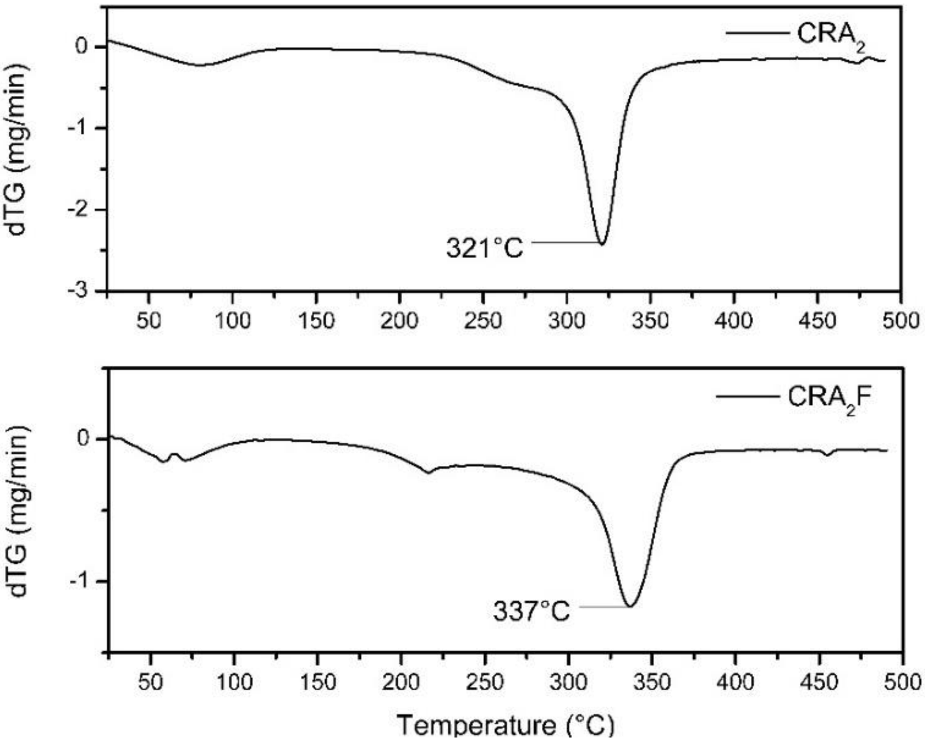

Figure 17 TGA curves of CRA_2 and CRA_2F samples.

On the other hand, similar to the CRA_2, the first and second stages of degradation in the CRA_2F sample, identified in the thermogram shown in **Figure 17**, correspond to the release of absorbed water in the range of 50-120 °C, and hemicellulose decomposition. The main stage of degradation is due to cellulose depolymerization and occurs at higher temperature (337°C) respect to that identified for the CRA_2 sample, this shift in the decomposition temperature suggest that CRA_2F presents a structure thermally more stable than CRA_2. This increase in thermal stability could be due to the fact that the CRA_2F sample has been really chemically modified with the use of thiourea, or that the crystallinity in both samples (CRA_2 and CRA_2F) was different. In addition, in the thermogram, it can see a peak at 216 °C, which is attributed to the decomposition of thiourea[80]. The last stage is the degradation of lignin, it usually occurs at temperatures higher than 500 °C[77], but due to the conditions of analyses, this peak is not shown.

3.2.6 X-Ray Diffraction

As it can see in **Figure 18**, all the diffractograms show a strong peak at a 2θ value of 22° and other peaks at 15°, 16°, and 34°. According to the literature, the signals that appear at 2θ = 22° correspond to the crystallographic plane (002), the signal at 15° is attributed to the plane (101), the signal at 16°, which is most noticeable in CS sample, is assigned to the plane ($10\bar{1}$). Finally, the signal at 35° is due to the plane (040). These planes are characteristic of cellulose type I. Furthermore, it was observed that the peaks of the prepared cellulose samples are wider than in the standard one, it could be associated not only with a contribution from the amorphous part but also with non-uniform strain within the crystal or differences in the crystallite size[81,82].

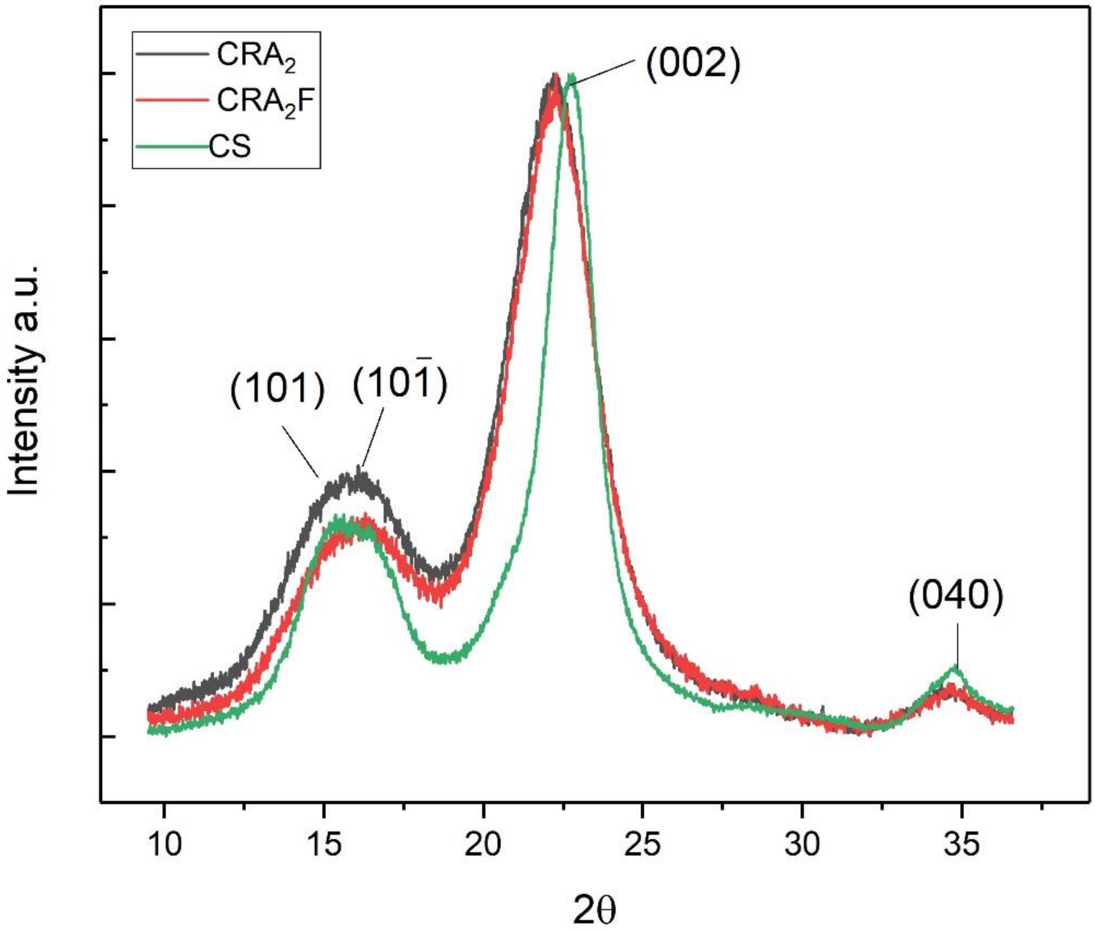

Figure 18 Diffractograms of CS, CRA$_2$, CRA$_2$F samples.

The XRD analysis allowed to evaluate the crystallinity index (CrI) of cellulose fibers in CS, CRA$_2$. and CRA$_2$F samples. The CrI values were calculated using the peak height (or intensity) method and applying the **Eq. 6** indicated above, and the obtained values are summarized in **Table 10**. These values are higher compared with those reported in the literature, this difference could be associated with the fact that the used method overestimated the calculate crystallinity values[81]. The crystallinity in cellulose fibers is due to intermolecular and intramolecular hydrogen bonds through hydroxyl groups[18]. If the amorphous phases were removed; those associated with cellulose structure itself or with other structures such as lignin or hemicelluloses, the CrI would increase. It was observed that CRA_2 and CRA_2F have similar crystallinity indices and differ from the value of standard cellulose. This demonstrates that the decomposition temperature shift for CRA_2F sample evidenced by TGA is due to the chemical modification in cellulose structure and not to the difference in its crystallinity.

Table 10 CrI % values of different cellulose samples

Samples	Crystallinity Index (%)
CS	88
CRA_2	75
CRA_2F	77

3.2.7 X-ray Photoelectron Spectroscopy (XPS) Analysis

In order to confirm the chemical structure of CRA_2 and CRA_2F samples, XPS analysis was performed, and the resultant spectra are shown in **Figure 19**. In can be noted that the peaks related to C 1s, O 1s and N 1s appear in both survey spectra. The signal of carbon and oxygen is associated with the structure of cellulose itself. Initially, the nitrogen peak should not be present in the CRA_2 sample, but its presence can be due to the use of nitric acid in the extraction process, being a source of nitrogen in the reaction medium that was incorporated into the cellulose structure. In addition, the use of thiourea in the CRA_2F sample causes that new signal corresponding to S 2p appears and that the nitrogen signal presents additional contributions. Each region of spectra is explained in detail below.

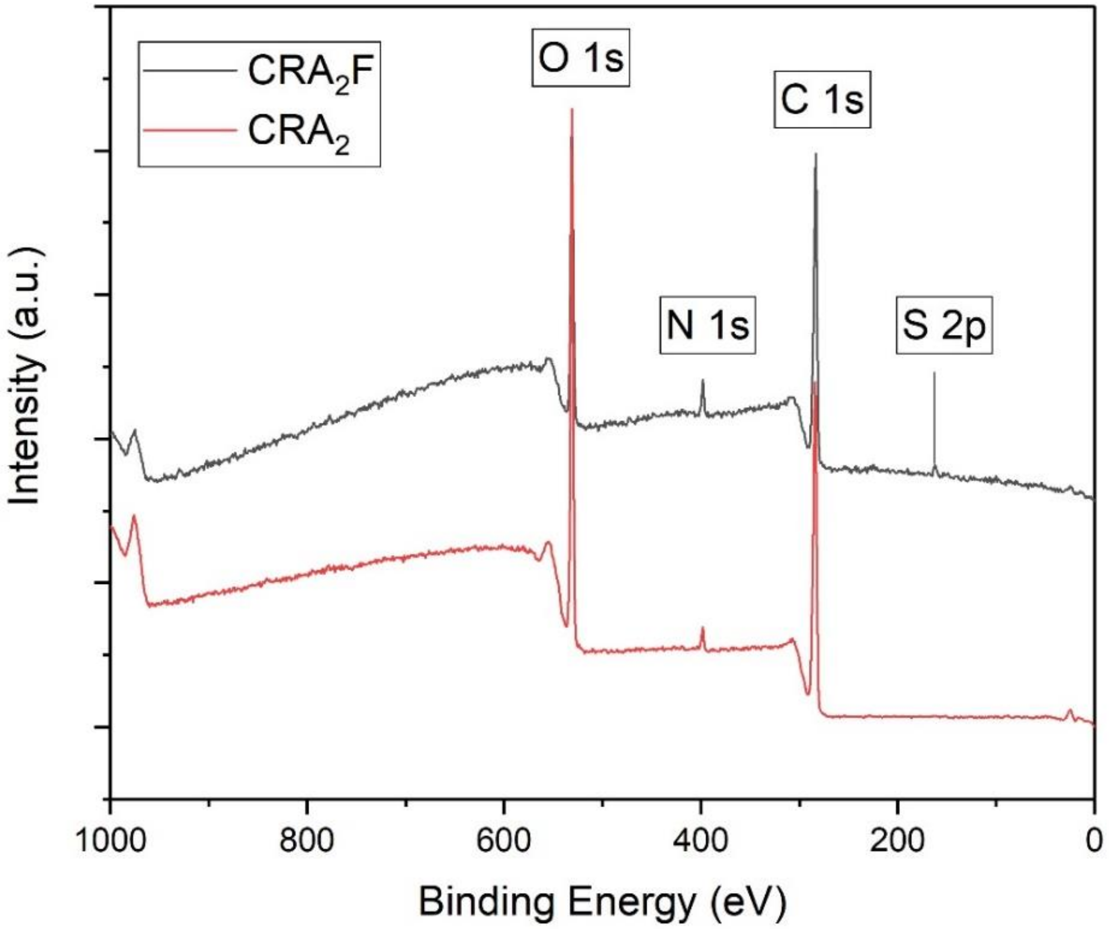

Figure 19 XPS surveys of CRA$_2$ and CRA$_2$F samples.

C 1s XPS spectrum of CRA$_2$ sample is illustrated in **Figure 20**, it shows four important peaks, the first one at 284.9 eV corresponding with C-H or C-C groups, it appears at the lowest binding energy, the second one at 286.3 eV is attributed to C-O group, the third peak is due to O-C-O or C=O groups at 287.7 eV, and the last one corresponds to O-C=O at 288.9 eV in an ester group. These signals are consistent with the information obtained from the characterization techniques mentioned above, which confirmed the esterification of the cellulose[83]. The modification process appears to be consistent with a Fischer esterification, which proceeds by the reaction between a carboxylic acid and an alcohol in the presence of a catalyst, under reflux, to form an ester[84]. In this project was used HNO_3 as the catalyst. The final structure of the cellulose after the esterification process, that is, the esterified cellulose, is proposed to be that shown in **Figure 21**.

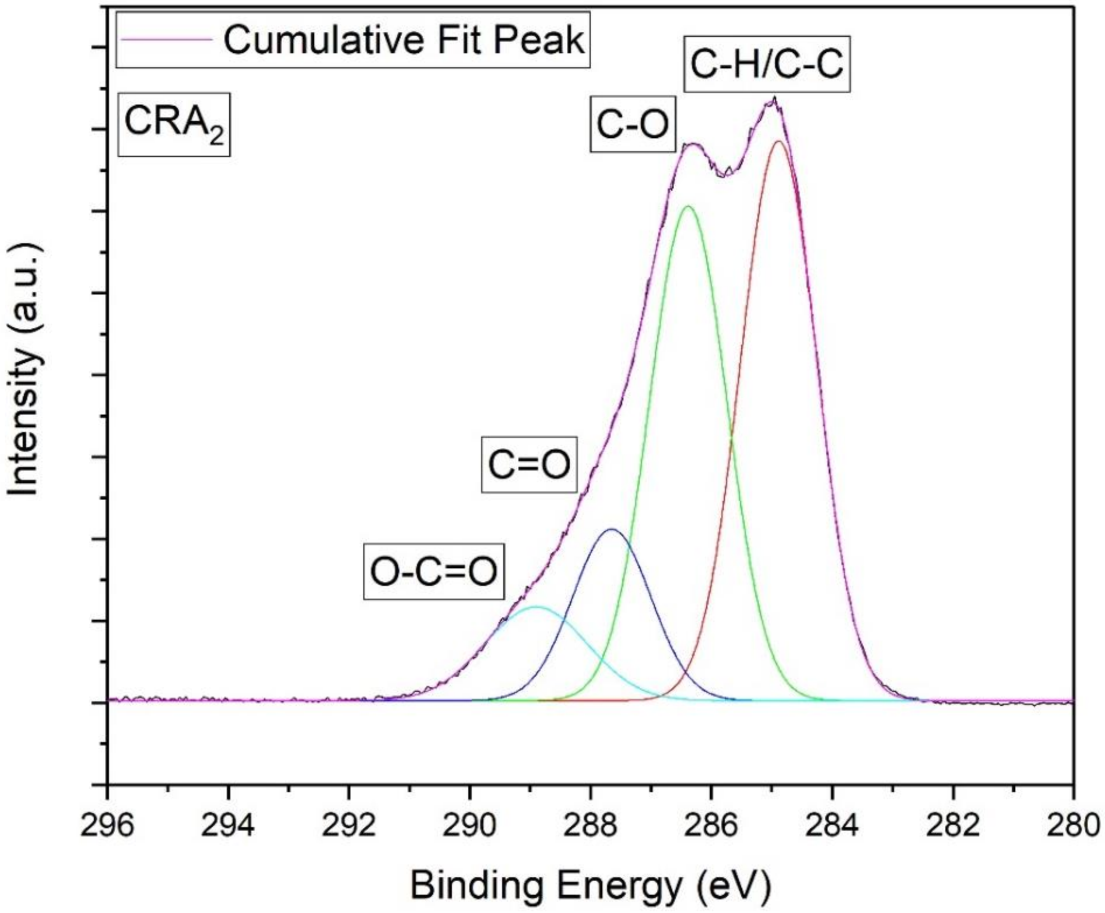

Figure 20 C 1s XPS spectrum of the CRA$_2$ sample.

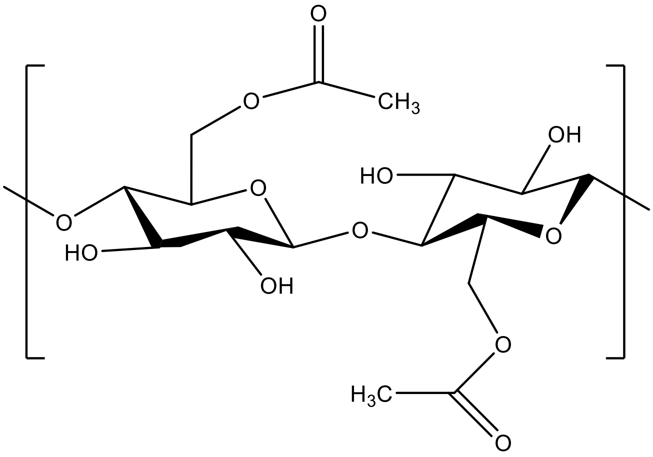

Figure 21 Proposed structure of esterified cellulose.

On the other hand, the CRA_2F XPS spectrum in the carbon region shows additional two peaks at 287.1 and 287.9 eV indicating the introduction of C-N and C=S groups[85,86], respectively, as it can see in **Figure 22**. These signals are consistent with the information provided by the FT-IR spectrum for CRA_2F, in which the presence of signals related to the mentioned bonds was evidenced. The obtained spectra in the nitrogen region, showed in **Figure 23** for both samples, it can be observed a strong peak at 398.5 eV for the CRA_2 case due to N-O group associated with the use of HNO_3 in the extraction process, and for CRA_2F an additional contribution at 400.3 eV due to C-N group of the thiourea attached was observed[86]. Finally, as was expected, the XPS spectrum of the CRA_2F sample shows only one peak in the sulfur region located at 162.1 eV [87,88], as it can see in **Figure 24**.

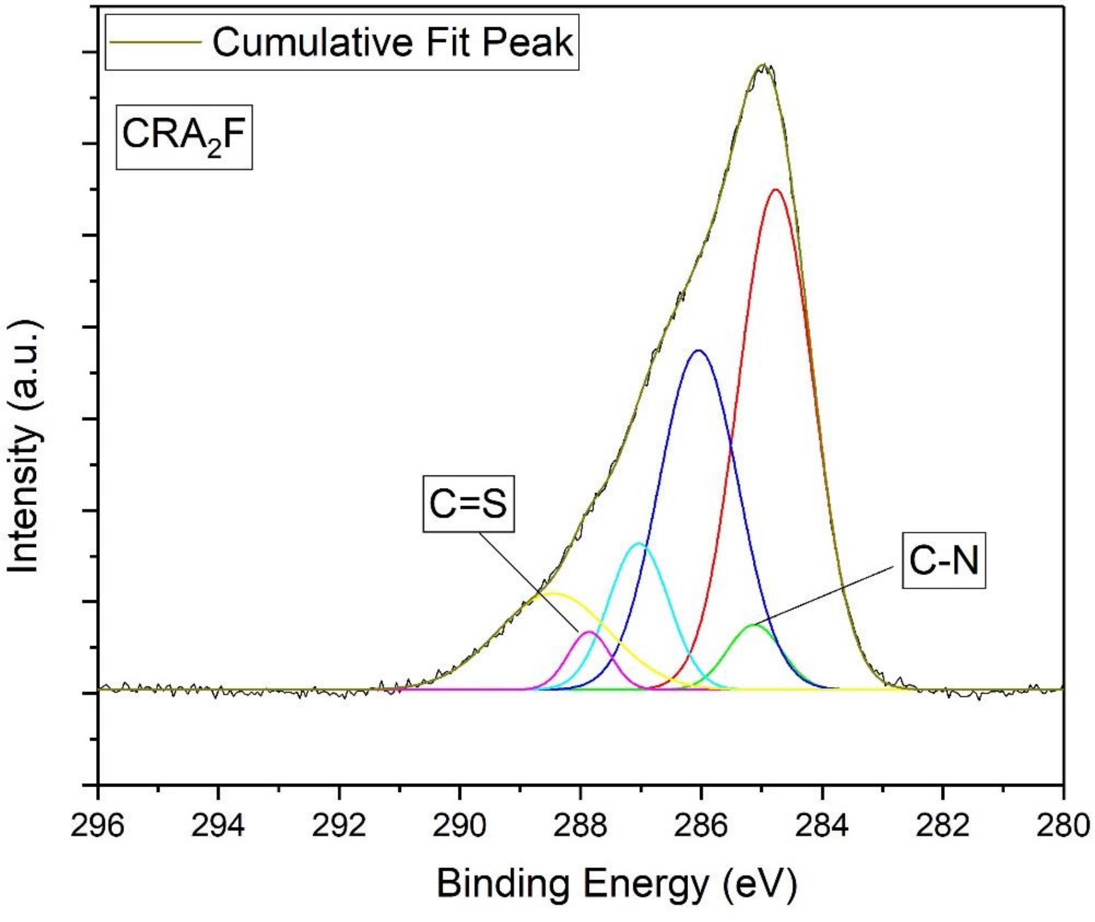

Figure 22 C1s XPS spectrum of CRA_2F sample.

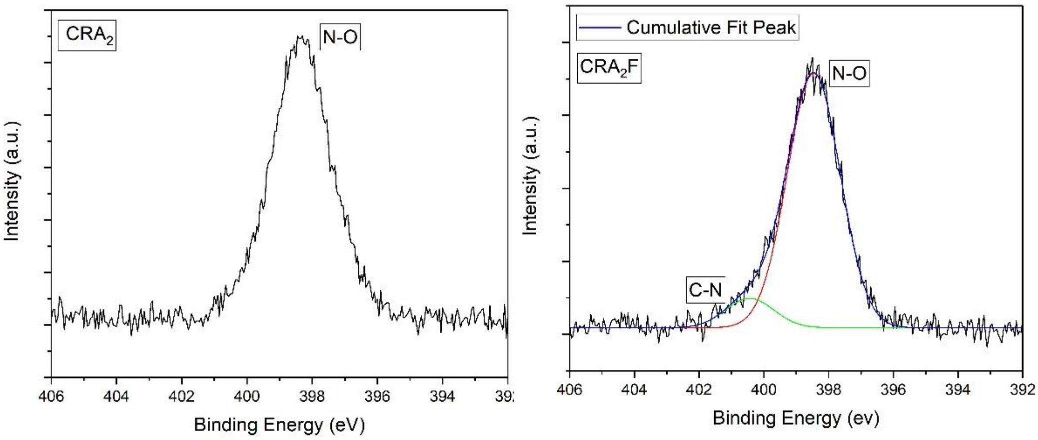

Figure 23 N 1s XPS spectrum of CRA_2 and CRA_2F samples.

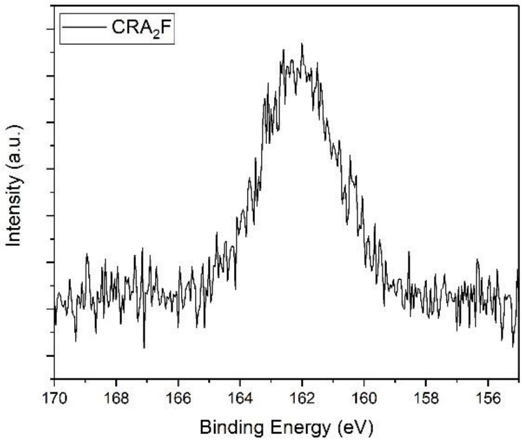

Figure 24 S 2p XPS spectrum of CRA_2F sample.

Only with the results obtained from different analyzes carried out, it was not possible to determine the final structure for CRA_2 after the incorporation of thiourea, that is for CRA_2F. However, the different analyzes carried out seem to indicate that the binding of thiourea to cellulose was through the nitrogen atom of the thiourea amino group, since are the signals associated with the nitrogen-containing groups those presented the most modifications in both FT-IR and XPS analyses, with respect to assignments for CRA_2 and with the values presented in the literature.

3.3 Ni(II) Calibration Curve construction

The Ni(II) calibration curve shown in **Figure 25** was constructed from $Ni(NO_3)$ standard solution with concentration ranged from 1 ppm to 10 ppm. For each standard solution, its absorbance was measured three times and these values were finally plotted. For the linear fit of these data, whose parameters are given in the inset of **Figure 25**, Pearson's coefficient (R-square) obtained showed a good value. The intercept and the slope values allow estimating the concentration of the nickel (C) in the solution associated to absorbance (Abs) value measure, using the following equation.

$$Abs = -0.03567 + 0.32454\,C \qquad \textbf{(8)}$$

Furthermore, the limit of detection (LoD) and the quantitation limit (LoQ) were calculated using **Eq. 11** and **Eq. 12** described in Annex E, which resulted in values 0.158 (mg/L) and 1.041 (mg/L), respectively. These values allowed to explore low nickel concentration values.

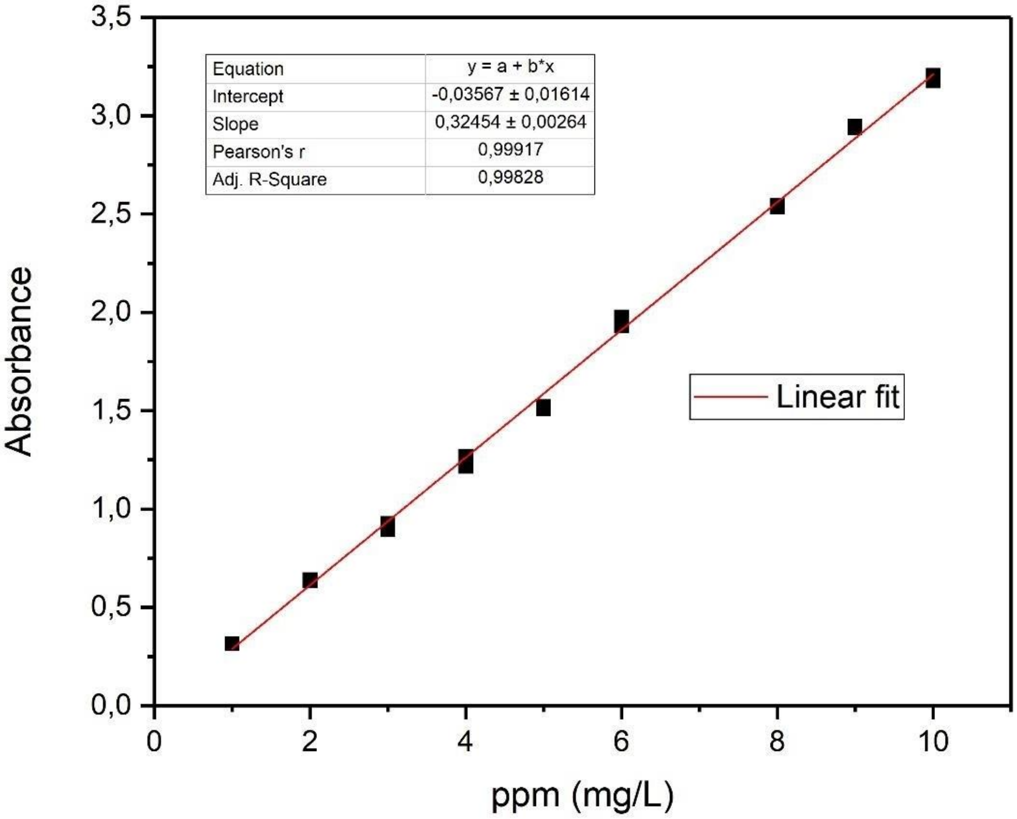

Figure 25 Calibration curve of Ni(II) using concentration from 1ppm to 10 ppm.

3.4 Adsorption process using cellulose-based adsorbents

3.4.2 Preliminary results of adsorption

Preliminary adsorption tests were performed using CS, CRA_2 and CRT samples, for which the initial concentrations of Ni(II) in solution was varied, while the amount of adsorbent remained constant. For the case of CS, the results after maintaining the adsorption process for one hour were not favorable, since the difference between initial

Ni(II) concentration and the final equilibrium Ni(II) concentration was very small. In this case, the method used was not able to detect such variation, so that the adsorption percentages are practically nil.

CRT and CRA_2 were the only samples that showed appreciable Ni(II) adsorption values, which are shown in **Table 11**. Although the CRT sample showed higher adsorption percentages than CRA_2, it was decided to continue working only with the CRA_2 sample because its extraction procedure has a lower environmental impact and its replicability is more affordable. In subsequent tests, the behavior of the adsorbent was evaluated by varying the parameters proposed in the preliminary studies. In addition, the CRA_2 sample also was treated with an organosulfur compound, which is thiourea, in order to modify the chemical structure of cellulose with the purpose of increasing the adsorption capacity of the sample. The analysis of CRA_2 and CRA_2F involved the use of techniques such as ^{13}C NMR, TGA, SEM, and XPS, detailed above in **Section 3.2.**

Table 11 Preliminary results of Ni(II) adsorption test using CRT and CRA_2 as adsorbents

	CRT			**CRA_2**		
Ni(II) Initial amount (mg)	Ni(II) Final amount (mg)	Ni(II) Adsorbed amount (mg)	% Ni(II) Adsorption	Ni(II) Final amount (mg)	Ni(II) Adsorbed amount (mg)	% Ni(II) Adsorption
5.0695	3.2793	1.7901	35.3119	4.7052	0.36433	7.18670
2.0763	1.0189	1.0574	50.9249	1.6589	0.41743	20.1038
1.2384	0.4000	0.8383	67.6956	0.7923	0.44615	36.0246

3.4.3 Adsorption of Ni(II) using CRA_2 and CRA_2F samples.

The absorbance values of each Ni(II) solution after contact with CRA_2 and CRA_2F and other important data are specified in **Table 12** and **Table 13**, the errors associated with these measures were found by applying the equations specified in Annex E. In this tests, the adsorbent mass was varied, in order to determine the amount of adsorbent necessary to achieve the best removal of the metal in solution, and the initial concentration of Ni(II) solution remained constant. After the nickel solution and adsorbent were in contact during 48 h, the concentration of the metal in the equilibrium (C_e) was obtained by measuring the absorbance of the resulting solution (after it was separated from the solid) and using the **Eq. 8** to find the correspondence between absorbance values and the concentration of the nickel in solution.

In addition, it can be seen that the greater the amount of the adsorbent, the greater the amount of Ni(II) adsorbed. Furthermore, despite the use of thiourea to increase the adsorption capacity of the adsorbent, there is no improvement of Ni(II) adsorption by CRA_2F. The $\mathbf{q_e}$ variable shown in **Table 12** and **Table 13** refers to the adsorbed amount of Ni(II) per mass unit of the adsorbent.

Table 12 Data corresponding to adsorption of Ni(II) using CRA_2 as adsorbent, evaluated at room temperature during 48 h. The initial concentration of the nickel solution was 51.1 mg/L, corresponding to an initial nickel mass of 1.278 mg.

CRA_2 mass ± 0.1 (mg)	Absorbance ±0.0001	**Ce** ± 2 (mg/L)	Nickel mass in solution (mg)	Adsorbed nickel mass (mg)	Adsorption Capacity, $\mathbf{q_e}$ (mg/g)	Adsorption Percentage (%)
15.1	1.5120	48	1.1922	0.0858	5.7215	6.7
50.2	1.3064	41	1.0338	0.2442	4.8835	19.1
75.5	1.1974	38	0.9499	0.3281	4.3752	25.7
100.1	1.1363	36	0.9028	0.3752	3.7518	29.4
125.1	1.0548	34	0.8400	0.4380	3.5037	34.3
150.1	0.9788	31	0.7815	0.4965	3.3102	38.9
350.1	0.8287	27	0.6658	0.6122	1.7491	47.9

Table 13 Data corresponding to Ni(II) adsorption using CRA_2F as adsorbent, evaluated at room temperature during 48 h. The initial concentration of the nickel solution was 51.1 mg/L, corresponding to an initial nickel mass of 1.278 mg.

CRA_2F mass ± 0.1 (mg)	Absorbance ±0.0001	**Ce** ± 2 (mg/L)	Nickel mass in solution (mg)	Adsorbed nickel mass (mg)	Adsorption Capacity, $\mathbf{q_e}$ (mg/g)	Adsorption Percentage (%)
50.2	1.2702	40	1.0059	0.2721	5.4418	21.29
75.4	1.2024	38	0.9537	0.3243	4.3238	25.37
100.3	1.0931	35	0.8695	0.4085	4.0852	31.97
125.3	1.0222	33	0.8149	0.4631	3.7048	36.24
150.1	0.9889	32	0.7892	0.4888	3.2583	38.24

It can be noticed that the nickel adsorption does not change notably for the different cellulose-based adsorbents. This means that the structural modification of cellulose did not contribute significantly to the nickel adsorption process, at least for the experimental conditions tested.

3.4.4 Adsorption Isotherms

The adsorption capacity can be evaluated by isotherms of adsorption, which are widely employed for fitting the obtained data using a representation of the adsorbed amount of nickel. As already mentioned, the isotherm of adsorption is expressed as milligrams of adsorbed nickel per mass unit of adsorbent (q_e) as a function of the equilibrium concentration of nickel in solution (C_e). Some models of isotherm of adsorption have been proposed, and the more convenient to represent the adsorption process depends on the composition and structure of adsorbent, that condition the nature of the interaction between adsorbate and adsorbent.

As an initial point in the evaluation of the adsorption process, it is worth mentioning that the percentage of Ni(II) removed from the solution proportionally increased with the mass of adsorbent for both the CRA_2 and CRA_2F samples. This occurred because the available surface for adsorption is larger, implying the presence of more active sites on which the metal can be adsorbed. However, different behavior can be observed for q_e, since this value decreases as the amount of adsorbent increased. This could be due to the fact that the adsorption capacity of CRA_2 was not fully exploited when the amount of the adsorbent was higher, that is, still there were active sites available for adsorption, implying a decrease in q_e. On the contrary, for the lower values of adsorbent mass, the surface tends to saturate rapidly, therefore, q_e increases[89].

The results obtained after the Ni(II) adsorption process were analyzed through the Langmuir and Freundlich models trying to evaluate the adsorption process involved. These two non-linear fits are shown in **Figure 27** along with the obtained data, and it can be noticed poor fits for both models. However, the situation changes if it is assumed that some different mechanism is involved for concentrations less than 23 ppm of nickel for the CRA_2 adsorbent, and from that value, the Langmuir model is better suited to experimental data. The same approximation can be applied to the fit for the case of CRA_2F samples but the displacement of the concentration is made up to 27 ppm. Langmuir isotherms with these displacements in the nickel concentration are represented in **Figure 26**.

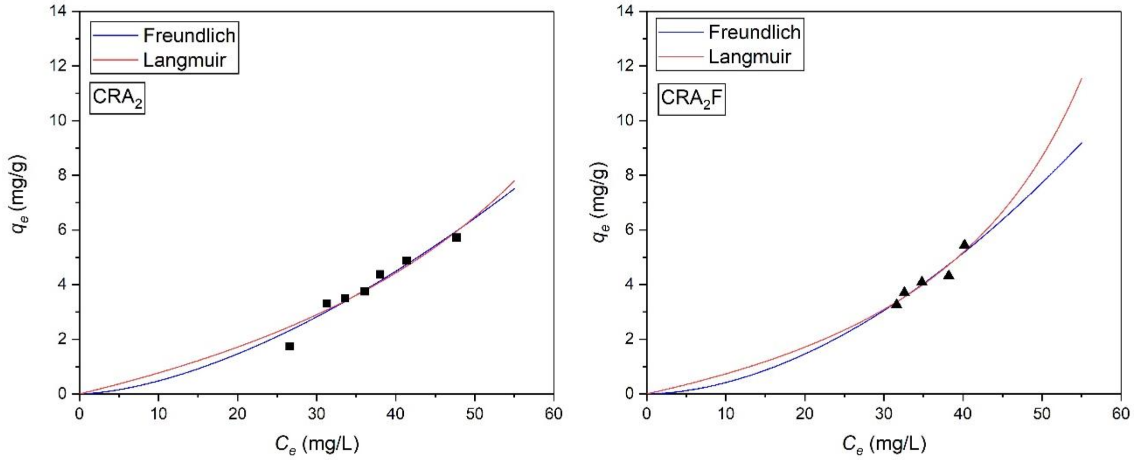

Figure 27 Nonlinear fit of Freundlich and Langmuir isotherms applied to CRA_2 and CRA_2F adsorption data.

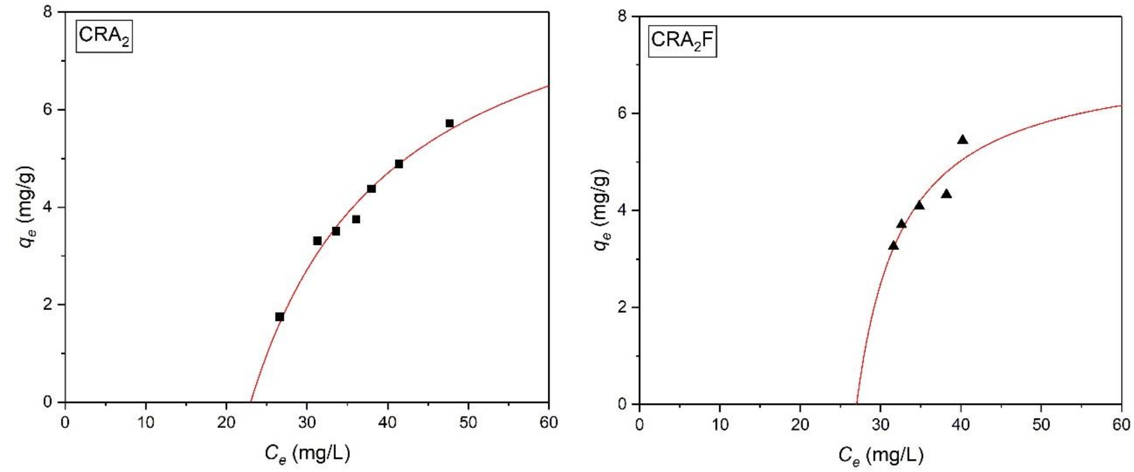

Figure 26 Langmuir isotherm applied **to** CRA_2 and CRA_2F adsorption data with suitable displacement in the Ni(II) concentration.

Considering the assumption mentioned above valid, Langmuir model seems to better describe nickel adsorption on the CRA_2 and CRA_2F samples, although for the last case it is less satisfactory. As additional information, it may be convenient to mention that the extrapolation of fits for Langmuir model to concentration values at which the saturation of monolayer is reached, reveals that the values analyzed in this work correspond to very low values, far from the saturation region. These extrapolations of the Langmuir model for both CRA_2 and CRA_2F are shown in **Figure 28**. From these fits of the Langmuir model, it is possible to estimate some characteristics of adsorbent, as for example the adsorbent amount required to completely cover the surface by the formation of a monolayer ($\boldsymbol{Q_0}$), as well as the equilibrium constant ($\boldsymbol{K_L}$) associated with the adsorption process analyzed. The values for these parameters are given in **Table 14**.

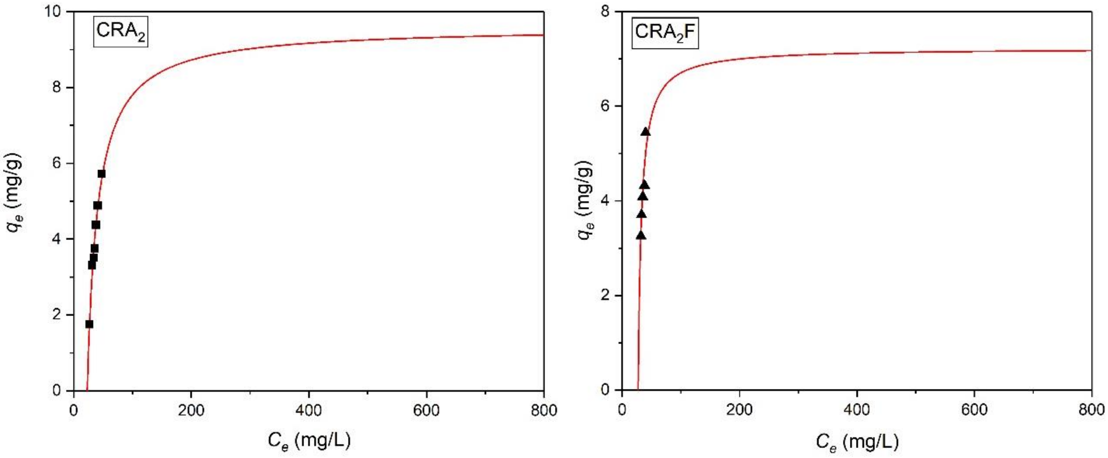

Figure 28 Extrapolation of the Langmuir isotherm for CRA$_2$ and CRA$_2$F data.

Table 14 Langmuir model parameters for CRA$_2$ and CRA$_2$F

Sample	Langmuir model parameters	Obtained values
CRA$_2$	$\boldsymbol{Q_0}$	9.6 mg/g
	$\boldsymbol{K_L}$	0.056 L/mg
CRA$_2$F	$\boldsymbol{Q_0}$	7.23 mg/g
	$\boldsymbol{K_L}$	0.175 L/mg

Deviations of the Langmuir model from the experimental data suggest heterogeneity in the energy of the adsorbent surface, therefore, the possibility of physisorption in certain areas of the fibers, in addition to chemisorption, is not ruled out. The physisorption process can be justified by the fact that the Freundlich model fits relatively well for experimental data, as can be seen in **Figure 27**.

According to literature, nickel behaves as a soft or hard acid, so it has the ability to form bonds with S, N or O, with which Ni(II) preferably forms octahedral or tetrahedral complexes[90]. However, CRA$_2$ did not show a high adsorption capacity which may be related to the fact that the acetylation in the sample was not complete, and as for the CRA$_2$F sample, the low thiourea concentration incorporated in it could affect significantly to the adsorption capacity of this sample. In **Table 14** are shown the obtained values for the equilibrium constant ($\boldsymbol{K_L}$) of the adsorption process and the maximum adsorption capacity ($\boldsymbol{Q_0}$) for both CRA_2 and CRA_2F determined by fits of Langmuir model. These values indicate that the CRA_2 sample has a slightly higher capacity of nickel adsorption, while the CRA_2F, due to its higher $\boldsymbol{K_L}$, showed a stronger interaction between nickel and species on the surface of the cellulose sample.

After being in contact with nickel solutions, both CRA_2-Ni and CRA_2F-Ni were studied by XPS, whose spectra can be seen in **Figure 29**. Unfortunately, the characteristic peaks associated with the presence of the nickel were not appreciable, this could occur since the amount of nickel in the sample subject to the analysis was less than 0.1%. However, there are slight displacements of the peaks in the oxygen region for samples containing nickel, as it can see in **Figure 30**, therefore, changes in the chemical environment of oxygen could be assumed due to the presence of nickel in the cellulose structure, suggesting a possible chemisorption.

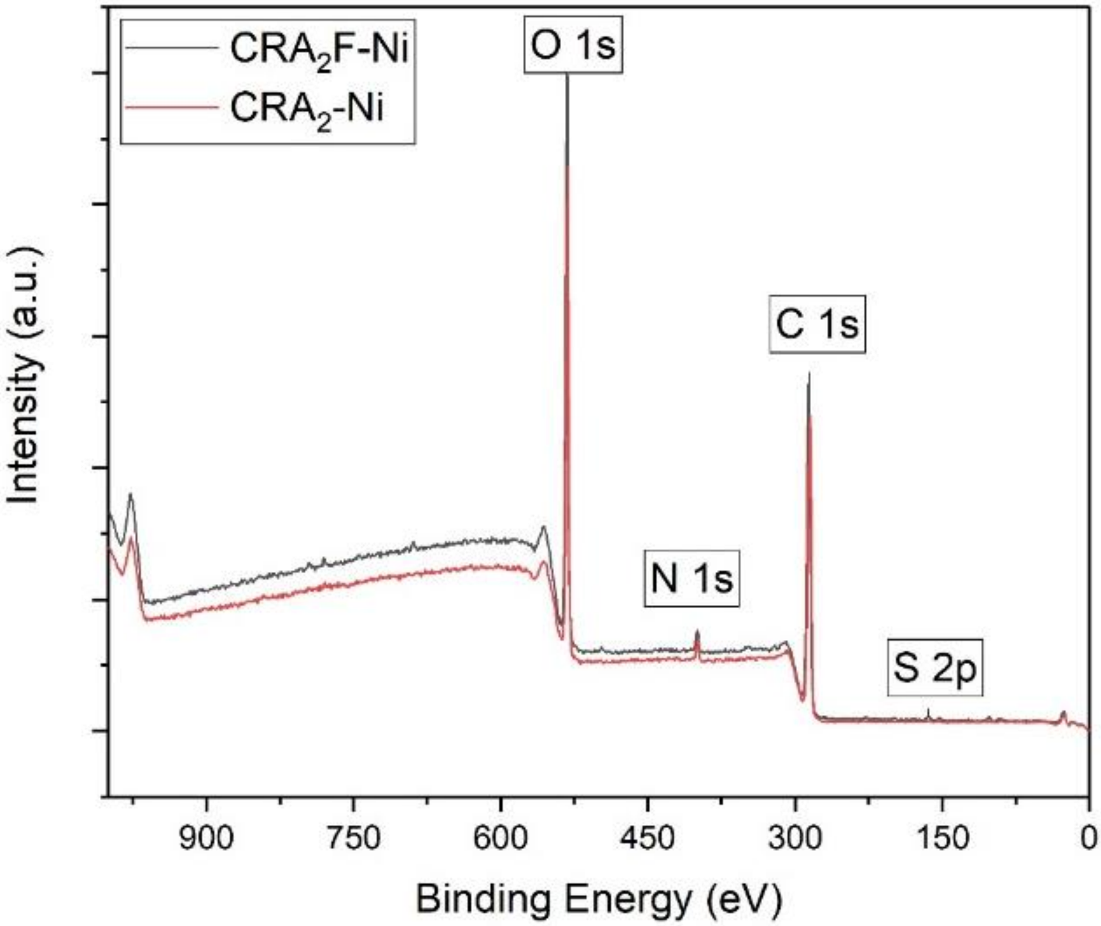

Figure 29 XPS Surveys of CRA_2 and CRA_2F after contact with the Ni (II) solution.

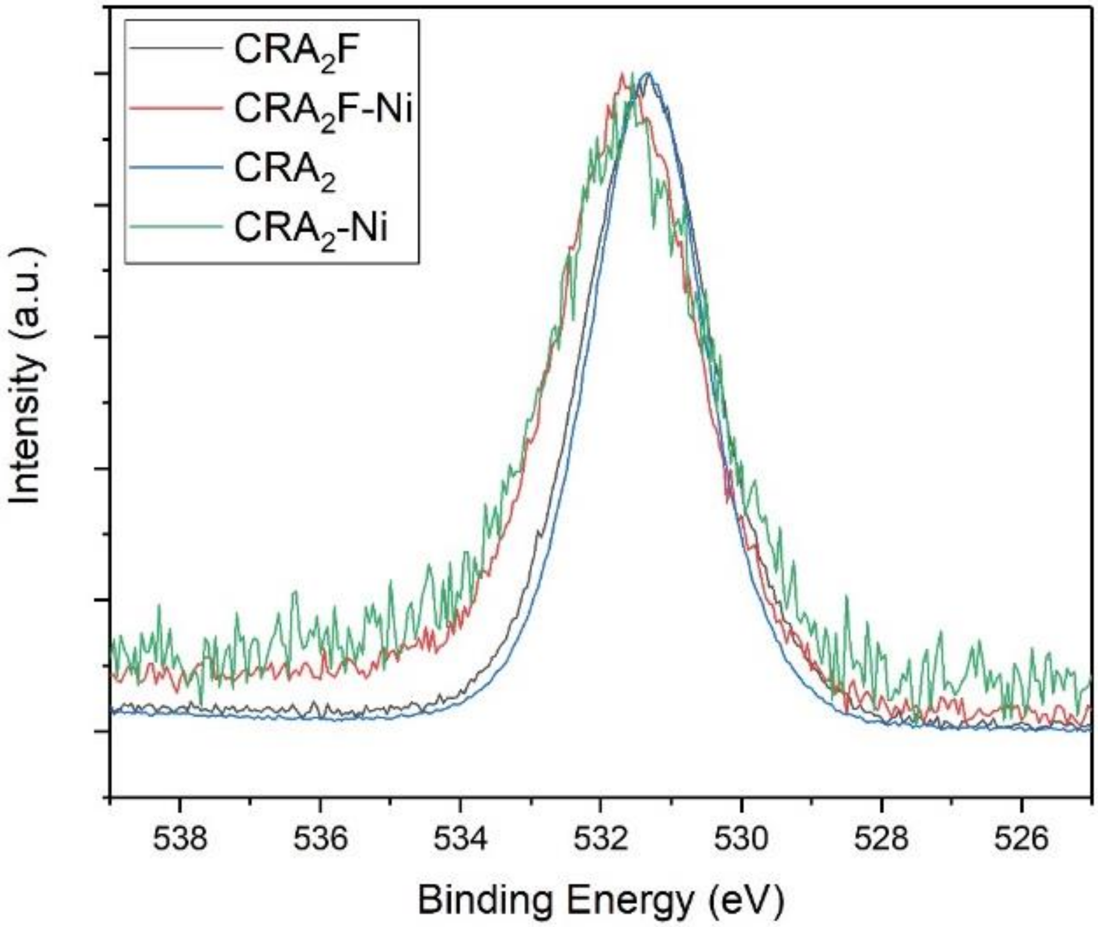

Figure 30 Oxygen region of the samples before and after contact with Ni(II).

3.5 Applicability

According to the studies carried out and the characteristics that the prepared solid shows, the installation of this bio adsorbent is proposed in the stage corresponding to the filtration, as can be seen in **Figure 31**. Usually, the water treatment plants are equipped with suitable sand filters[91], the idea is to include a new layer that contributes to the effective elimination of remnants of potentially toxic metals. However, the developed adsorbent must continue even understudy, especially if it is necessary to increase its efficiency in terms of metal capture in the shortest possible time and its potential implementation at the industrial level.

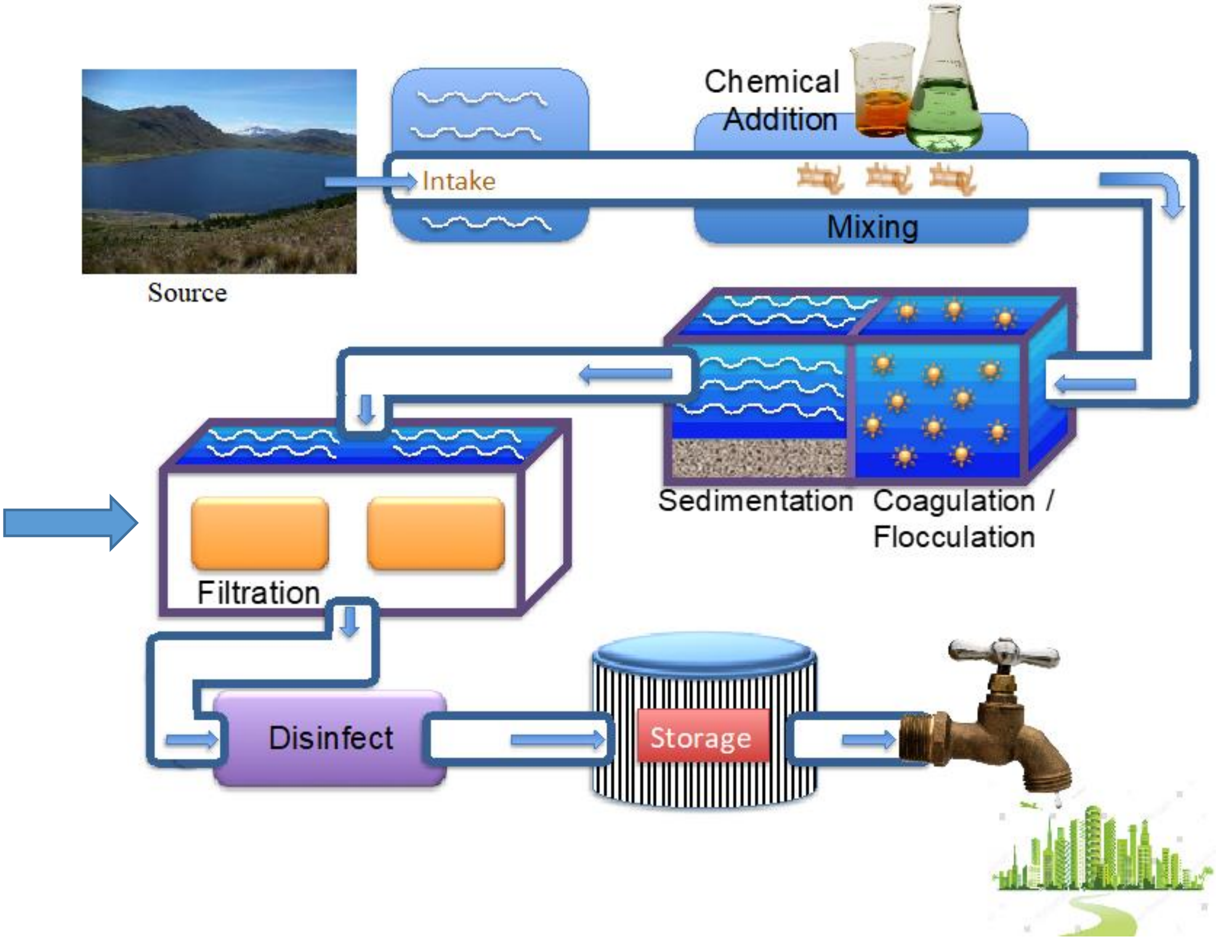

Figure 31 Scheme of the application of the bio adsorbent in a water treatment plant.

CHAPTER IV

CONCLUSIONS AND RECOMMENDATIONS FOR FUTURE RESEARCH

CONCLUSIONS

- It was extracted cellulose from rose stems by two procedures, each one of them involving different extraction solvents, and in both cases was confirmed by FT-IR spectra the presence of lignin and hemicellulose that remain in the structure, noticing the appearance of the peaks corresponding to bonds vibrations that not are associated with cellulose, such as the C=C (1505 cm^{-1}), C-O (1260 cm^{-1}), and C-H (801 cm^{-1}) bonds. Furthermore, the presence of these species is also observed in the micrographs, provided irregularity to the surface of extracted cellulose.
- The two procedures used to obtain cellulose samples were compared in terms of productivity and environmental impact. It is suggested that the procedure executed to obtain CRA_2 sample corresponds to the one with the least impact on the environment without require a high number of treatments, unlike the procedure to obtain CRT, which involved the use of contaminating reagents and several steps. Therefore, it was decided to work with CRA_2 for further studies.
- Through the FT-IR, ^{13}C NMR, and XPS techniques the acetylation of the cellulose structure in CRA_2 was confirmed, and a Fischer esterification was suggested as a possible mechanism of reaction.
- TGA analyses showed that CRA_2F is more thermally stable than CRA_2, and because XRD analysis confirmed a similar crystallinity for both samples, this higher stability can be due to some change in the chemical structure.
- Through the gas adsorption technique, the textural properties of the solid were determined. According the textural analysis it was determined that CRA_2 and CRA_2F showed small specific surface area (S_{BET}) and very small pore size (D_p), so the samples are considered non-porous.
- Preliminary results obtained from adsorption tests showed that standard cellulose (CS) not present a notable capacity to adsorb Ni(II), at least the method of quantification used, based in the formation of the $[Ni(dmg)_3]^{2-}$ complex was not able to detect the small variation of nickel concentration during the adsorption process.

- The isotherms of Langmuir and Freundlich not fitted completely the experimental data obtained by Ni(II) adsorption test for CRA_2 and CRA_2F, however, with a little modification in Langmuir model a better fit was obtained.
- CRA_2 corresponds to a solid with a low adsorption capacity (q_e) to adsorb nickel from aqueous solutions, reaching a maximum adsorption percentage of 47.9% and a maximum adsorption capacity (Q_0) of 7.58 mg Ni(II)/$g_{adsorbent}$.
- Because the low percentage of thiourea incorporated to cellulose; that is in CRA_2F sample, its presence did not contribute significantly to improving the nickel adsorption.

RECOMMENDATIONS

- Study the behavior of the adsorbent by varying other parameters such as pH and temperature of nickel solutions.
- Improve the treatment of cellulose structure modification increasing the thiourea concentration or varying the pH of the medium, that could contribute to enhance the adsorption of metals.
- Direct the extraction process until obtaining of nanocellulose, evaluate its specific surface, and use it as a precursor of cellulose-based adsorbent.
- For the implementation of the solid studied as a bio adsorbent in a water treatment plant, it is necessary to evaluate its cost-benefit ratio.

ANNEXES

ANNEX A: Biomass Treatment and solid samples preparation

Rose stem

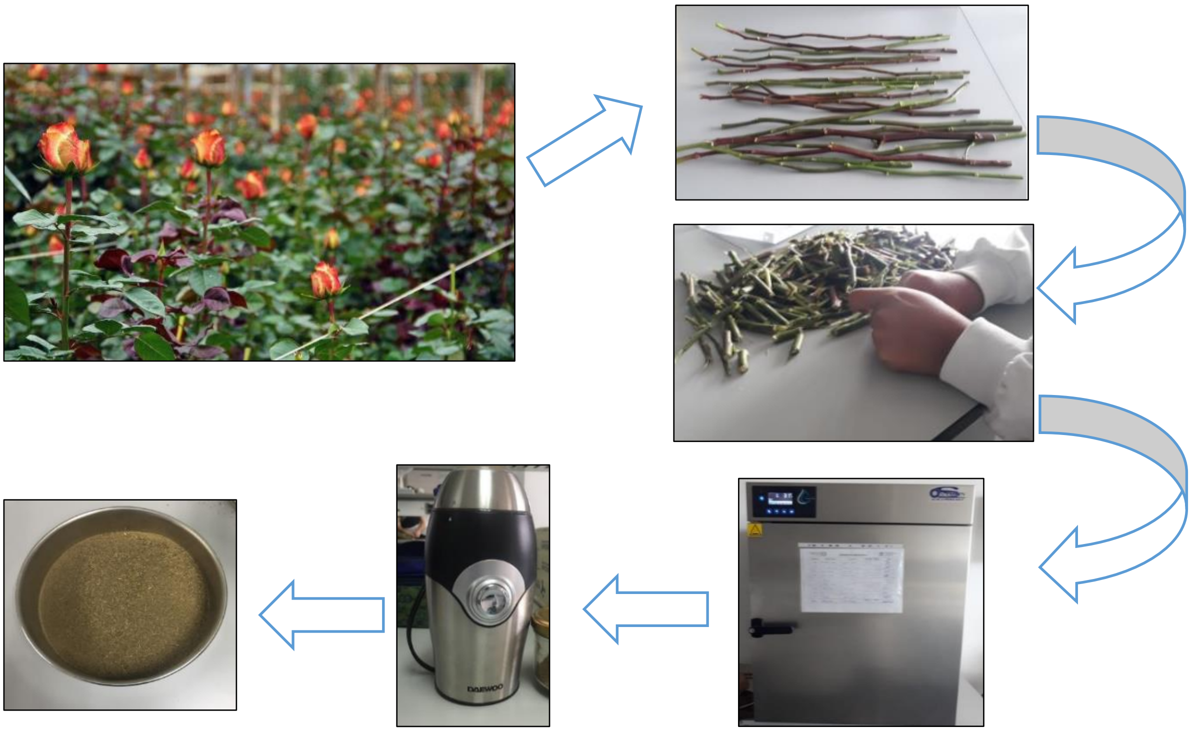

CRT preparation.

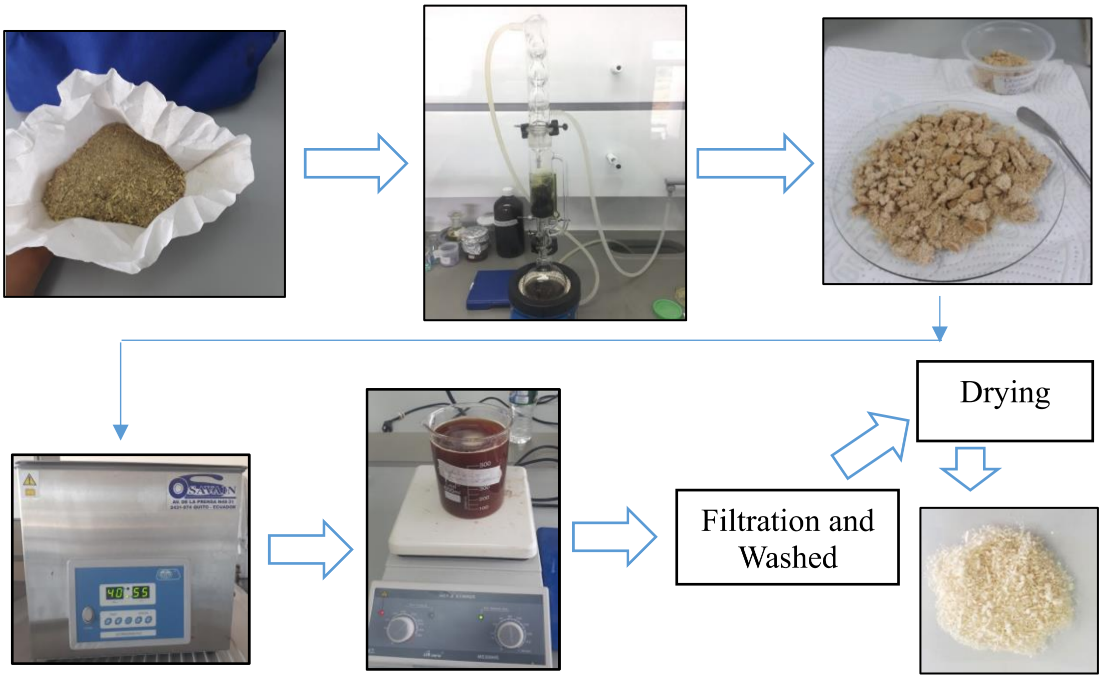

CRA$_2$ Preparation

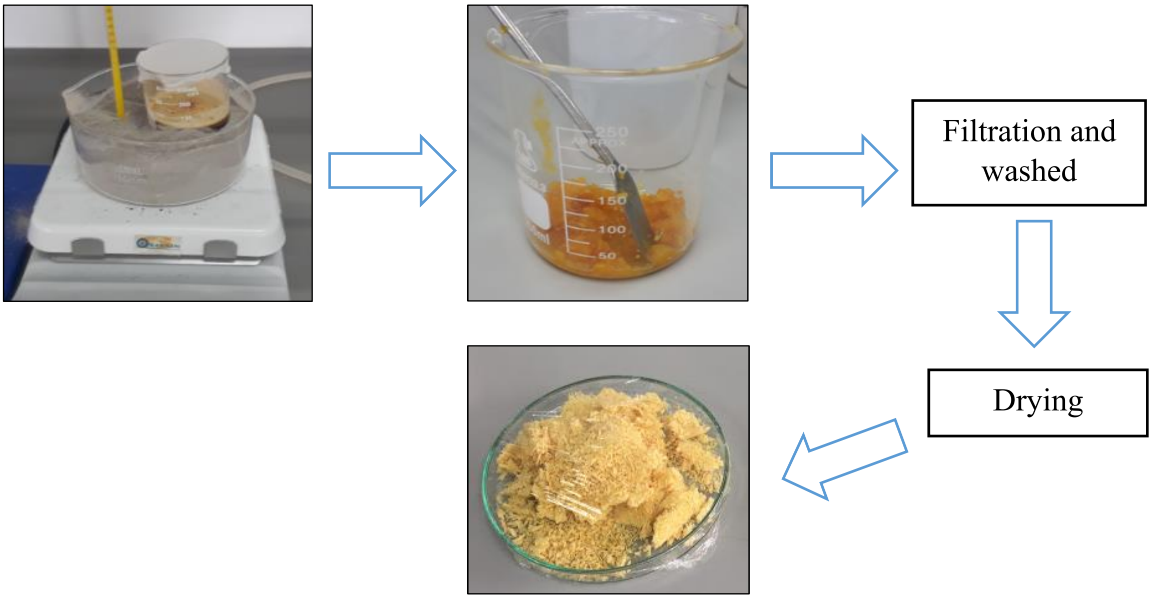

ANNEX B: Modification of the samples with thiourea

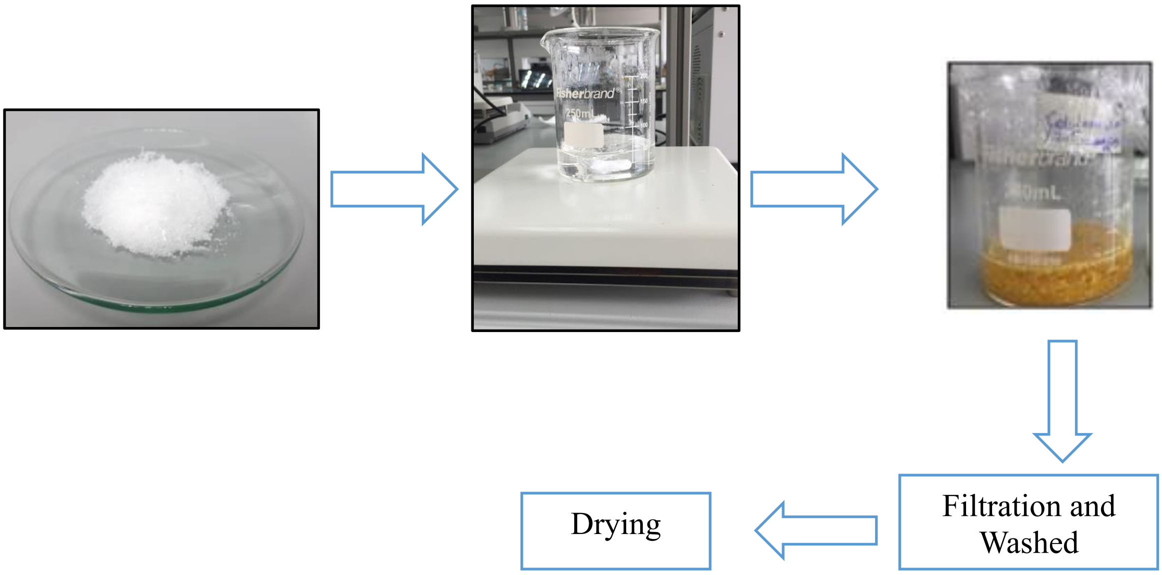

ANNEX C: Adsorption test of Ni(II) and complex formation

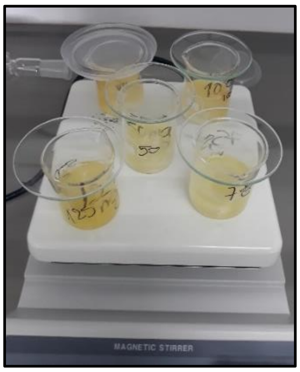

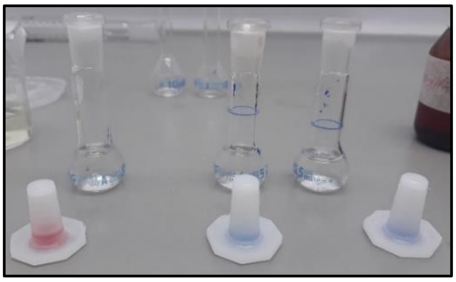

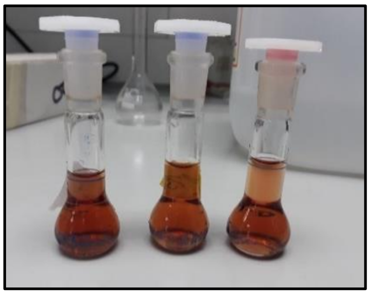

ANNEX D Used Reagents for each procedure.

	Reagents	Description	**Materials**
Solid preparation	Toluene	(C_7H_8) Reactivos RD COD: 220-2	Universal support and clamps
	Ethanol	(CH_3CH_2OH) N.S.	Soxhlet, round bottom flask (150 mL), condenser.
	Sodium Hydroxide	($NaOH$) AR® (ACS) CAS: 1310-732	Beakers (500, 200, 100 mL)
	Peroxide	30% (H_2O_2) Fisher Chemical CAS: 7722-84-1	Buchner, filter paper (4-12µm and 1-2µm)
	Distilled water	N.S.	Spatula, glass watch, glass rod
	Nitric Acid	65% (HNO_3) EMSURE® 1004562500	Hot plate, thermometer
	Acetic Acid (glacial)	100% (CH_3OH) EMSURE® 1000632500	Magnetic stirrers.
Functionalization of the solid.	Thiourea	(CH_4N_2S) 99% LOBA Chemie CAS: 62-56-6	Spatula, beaker (50 mL). glass watch
	Ethanol	(CH_3CH_2OH)	Container
Standard preparations and Adsorption test	Pure Nickel Strip	SIGMA-ALDRICH 99.95%	Volumetric pipette (25 mL), graduated pipette (1 mL, 5 mL), micropipettes (0.1-1mL and 0.5- 5mL) Pasteur pipette
	Nitric Acid	(HNO_3) 65% EMSURE® 1004562500	Beakers (50 mL). magnetic stirrers.
	Distilled water	N.S.	Filter paper (4-12 µm. 1-2 µm)
			containers
Bromine water synthesis and Dimethylglyoxime preparation	Potassium Bromide	KBr SIGMA-ALDRICH ≥99% CAS: 7758-02-3	Two necks round bottom flask. elbow. condenser
	Sulfuric Acid	H_2SO_4 BAKER®ACS 97.99% CAS:7664-93-9	Spatula. test tube. magnetic stirrers
	Hydrogen peroxide	30% H_2O_2	Hot plate
	Distilled water	N.S.	Erlenmeyer (250 mL)
	Dimethylglyoxime	$C_4H_8N_2O_2$ SIGMA-ALDRICH CAS: 95-45-4	Beaker (500 mL). test tube.
	Ethanol	(CH_3CH_2OH)	

Complex Formation	Bromine water		Graduated pipette (1 mL)
	Dimethyl glyoxime 1%		Micropipettes (P1000)
	Ammonium Hydroxide	NH_4OH Fisher Chemical CAS: 1336-21-6	Pasteur pipette
	Distilled water	N.S.	Volumetric flask (10, 50 mL)

ANNEX Errors calculation

The determination of the concentration of Ni(II) in solution is subject to error due to interpolation. **Eq. (9)** is used to determine it.

$$S_{x_o} = \frac{S_{y/x}}{b}\sqrt{\frac{1}{m}+\frac{1}{n}+\frac{(y_o-\bar{y})^2}{b^2\sum_i(x_i-\bar{x})^2}} \qquad \textbf{(9)}$$

In this equation. y_o is the experimental value of the absorbance from which the concentration value $x_0$is calculated, S_{x_o} is the estimated standard deviation of x_0, b is the value of the slope obtained in the calibration curve, m the number of times the absorbance was measured for each standard, n is the number of prepared standards, and $\bar{y}$ is the average of all absorbances measured, x_i is the concentration of the standard, and $\bar{x}$ is the average of the concentrations[92]. Furthermore, the errors are also attributed to the use of the instrument, so, in order to calculate the global error, **Eq. (10)** corresponding to the propagation of errors will be used.

$$\frac{Sy}{y} = \sqrt{\left(\frac{Su}{u}\right)^2+\left(\frac{Sv}{v}\right)^2+\left(\frac{Sw}{w}\right)^2}\ . \qquad \textbf{(10)}$$

Confidence limits can be calculated as $x_0 \pm t_{(n-2)}S_{x_0}$. with (n -2) degrees of freedom[92]. The confidence level used will be 95% corresponding to a t-statistic value of 2.36. Furthermore, the limit of detection (LoD) is calculated as:

$$LoD = y_B + 3S_B\ , \qquad \textbf{(11)}$$

where y_B is the concentration giving a signal equal to the blank and S_B correspond to the standard deviations of the blank. Finally, the limit of quantification, defined as the lower limit for precise quantitative measurements[92] is calculated using **Eq. 12**

$$LoQ = y_B + 10S_{B\,.} \qquad \textbf{(12)}$$

Bibliography

(1) Zhou, Y.; Fu, S.; Zhang, L.; Zhan, H.; Levit, M. V. Use of Carboxylated Cellulose Nanofibrils-Filled Magnetic Chitosan Hydrogel Beads as Adsorbents for Pb(II). *Carbohydr. Polym.* **2014**, *101* (1), 75–82. https://doi.org/10.1016/j.carbpol.2013.08.055.

(2) William, D.; Connell, O.; Birkinshaw, C.; Francis, T.; Dwyer, O. Heavy Metal Adsorbents Prepared from the Modification of Cellulose : A Review. **2008**, *99*, 6709–6724. https://doi.org/10.1016/j.biortech.2008.01.036.

(3) Connell, D. W. O.; Birkinshaw, C.; Dwyer, T. F. O. A Modified Cellulose Adsorbent for the Removal of Nickel (II) from Aqueous Solutions. **2006**, *1828* (May), 1820–1828. https://doi.org/10.1002/jctb.

(4) Kosheleva, A.; Atamaniuk, I.; Politaeva, N.; Kuchta, K. Adsorption of Rare Earth Elements Using Bio-Based Sorbents. *MATEC Web Conf.* **2018**, *245*. https://doi.org/10.1051/matecconf/201824518001.

(5) Negrea, A.; Gabor, A.; Davidescu, C. M.; Ciopec, M.; Negrea, P.; Duteanu, N.; Barbulescu, A. Rare Earth Elements Removal from Water Using Natural Polymers. *Sci. Rep.* **2018**, No. 2, 1–11. https://doi.org/10.1038/s41598-017-18623-0.

(6) Berg, J. M.; Tymoczko, J. L.; Stryer, L.; Gregory, J.; Gatto, J. *Biochemistry*, 7th ed.; 2012.

(7) Fennema, O.; Tannenbaum, S. *Introducción a La Química de Los Alimentos*, 2nd ed.; 1993.

(8) Zhou, D.; Zhang, L.; Zhou, J.; Guo, S. Cellulose / Chitin Beads for Adsorption of Heavy Metals in Aqueous Solution. **2004**, *38*, 2643–2650. https://doi.org/10.1016/j.watres.2004.03.026.

(9) Kamel, S.; Hassan, E. M. Preparation and Application of Acrylonitrile-Grafted Cyanoethyl Cellulose for the Removal of Copper (II) Ions. **2005**, No. Ii. https://doi.org/10.1002/app.23317.

(10) Corporación Financiera Nacional (CFN). *Ficha Sectorial: Cultivo de Flores*; 2017.

(11) Hokkanen, S.; Bhatnagar, A.; Sillanpää, M. A Review on Modification Methods to Cellulose-Based Adsorbents to Improve Adsorption Capacity. *Water Res.* **2016**, *91*, 156–173. https://doi.org/10.1016/j.watres.2016.01.008.

(12) Sud, D.; Mahajan, G.; Kaur, M. P. Agricultural Waste Material as Potential Adsorbent for Sequestering Heavy Metal Ions from Aqueous Solutions - A Review. *Bioresour. Technol.* **2008**, *99* (14), 6017–6027. https://doi.org/10.1016/j.biortech.2007.11.064.

(13) EXPOFLORES. *Informe de Exportaciones de Rosas Tercer Trimestre 2018*; 2018.

(14) Rutkowski, P.; Waliszewska, B.; Mleczek, M.; Zborowska, M.; Golin, P.; Szentner, K. Changes in the Chemical Composition and the Structure of Cellulose and Lignin in Elm Wood Exposed to Various Forms of Arsenic. **2019**, *0123456789*, 6303–6315. https://doi.org/10.1007/s10570-019-02511-z.

(15) González-Velandia, K.-D.; Daza-Rey, D.; Caballero-Amado, P.-A.; Martínez-González, C. Evaluación de Las Propiedades Físicas y Químicas de Residuos Sólidos Orgánicos a Emplearse En La Elaboración de Papel. *Luna Azul* **2016**, *43* (43), 499–517. https://doi.org/10.17151/luaz.2016.43.21.

(16) Klemm, D.; Heublein, B.; Fink, H.; Bohn, A. Polymer Science Cellulose : Fascinating Biopolymer and Sustainable Raw Material Angewandte. **2005**, 3358–3393. https://doi.org/10.1002/anie.200460587.

(17) Nelson, D. L.; Cox, M. M. *Lehninger Principles of Biochemistry*, 6th ed.; 2013.

(18) Kayra, N.; Aytekin, A. Ö. Synthesis of Cellulose-Based Hydrogels : Preparation , Formation , Mixture , and Modification. **2018**. https://doi.org/https://doi.org/10.1007/978-3-319-76573-0_16-1.

(19) Watkins, D.; Nuruddin, M.; Hosur, M.; Tcherbi-Narteh, A.; Jeelani, S. Extraction and Characterization of Lignin from Different Biomass Resources. *J. Mater. Res. Technol.* **2015**, *4* (1), 26–32. https://doi.org/10.1016/j.jmrt.2014.10.009.

(20) Li, L.; Rowbotham, J. S.; Christopher Greenwell, H.; Dyer, P. W. *An Introduction to Pyrolysis and Catalytic Pyrolysis: Versatile Techniques for Biomass Conversion*; 2013. https://doi.org/10.1016/B978-0-444-53878-9.00009-6.

(21) Nunes, R. C. R. Rubber Nanocomposites with Nanocellulose. In *Progress in Rubber Nanocomposites*; Elsevier Ltd, 2017; pp 461–492. https://doi.org/10.1016/B978-0-08-100409-8.00013-9.

(22) Singha, A. S.; Guleria, A. International Journal of Biological Macromolecules Chemical Modification of Cellulosic Biopolymer and Its Use in Removal of Heavy Metal Ions from Wastewater. *Int. J. Biol. Macromol.* **2014**, *67*, 409–417. https://doi.org/10.1016/j.ijbiomac.2014.03.046.

(23) Chunilall, V.; Bush, T.; Tomas, P. Supra-Molecular Structure and Chemical Reactivity of Cellulose I Studied Using CP/MAS 13C-NMR. *Cellul. - Fundam. Asp.* **2013**. https://doi.org/10.5772/50673.

(24) CABALLERO, B. Encyclopedia of Food Sciences and Nutrition. *Encycl. food Sci. Nutr.* **2003**, *1* (9), 1689–1699. https://doi.org/10.1017/CBO9781107415324.004.

(25) Eriksson, H. Cellulose Reactivity - Difference between Sulfite and PHK Dissolving Pulps, Umeå University, 2014.

(26) Srivastava, A. K.; Pasala, R.; Minhas, P. S.; Suprasanna, P. *Plant Bioregulators for Sustainable Agriculture: Integrating Redox Signaling as a Possible Unifying Mechanism*; Elsevier Inc., 2016; Vol. 137. https://doi.org/10.1016/bs.agron.2015.12.002.

(27) Ziegler-Skylakakis, K.; Kielhorn, J.; Könnecker, G.; Koppenhöfer, J.; Mangelsdorf, I. Concise International Chemical Assessment Document 49: Thiourea. *IPCS Concise Int. Chem. Assess. Doc.* **2003**, No. 49.

(28) Ochiai, B.; Tsuda, K. Selective Capture of Pd2+ by Graft Copolymer Bearing LCST Graft Chain and Metal Adsorbing Stem Chain. *J. Polym. Sci. Part A Polym. Chem.* **2019**, *2*, 1–4. https://doi.org/10.1002/pola.29520.

(29) Li, X.; Tang, Y.; Cao, X.; Lu, D.; Luo, F.; Shao, W. Preparation and Evaluation of Orange Peel Cellulose Adsorbents for Effective Removal of Cadmium , Zinc , Cobalt and Nickel. **2008**, *317*, 512–521. https://doi.org/10.1016/j.colsurfa.2007.11.031.

(30) KAN Group. KAN-therm: Health risks caused by nickel connector in drinking water installations http://en.kan-therm.com/about/knowledge_base/articles/health_risks_caused_by_nickel_connector_in_drinking_water_installations.html (accessed Feb 26, 2020).

(31) Das, K. K.; Das, S. N.; Dhundasi, S. A. Nickel, Its Adverse Health Effects & Oxidative Stress. *Indian J. Med. Res.* **2008**, *128* (4), 412–425.

(32) Nordberg, G. F.; Fowler, B. a.; Nordberg, M. Handbook of The Toxicology of Metal. **2009**, 1024.

(33) INEN. *Norma Técnica Ecuatoriana - Agua Potable (INEN 1108: 2014-01)*; 2014; pp 1–10.

(34) Ministerio del Ambiente. *Anexo 1 Del Libro Vi Del Texto Unificado De Legislacion Secundaria Del Ministerio Del Ambiente: Norma De Calidad Ambiental Y De Descarga De Efluentes Al Recurso Agua*; 2014.

(35) Davis, D. G.; Boundreaux, E. A. Nickel(IV) Dimethylglioxime. *Electroanal. Chem.* **1964**, 434–441. https://doi.org/https://doi.org/10.1016/0022-0728(64)80082-6.

(36) Rath, M.; Behera, L. P.; Dash, B.; Sheik, A. R.; Sanjay, K. Hydrometallurgy Recovery of Dimethylglyoxime (DMG) from Ni-DMG Complexes. *Hydrometallurgy* **2018**, *176* (January), 229–234. https://doi.org/10.1016/j.hydromet.2018.01.014.

(37) Panda, R. K.; Acharya, S.; Neogi, G. Studies in Nickel(IV) Chemistry. Part 1. Preparation, Characterization, and Kinetics of Formation of Tris(Dimethylglyoximato)Nickelate(IV) in Aqueous Alkaline Media. *Chem. Soc. Dalt. Trans.* **1983**, No. 7, 1225–1231. https://doi.org/https://doi.org/10.1039/DT9830001225.

(38) Indira Gandhi National Open University (IGNOU). *Spectrophotometric Determination of Nickel Using Dimethylglyoxime.*

(39) Sahu, O.; Singh, N. *Significance of Bioadsorption Process on Textile Industry Wastewater*; Elsevier Ltd., 2018; Vol. 13. https://doi.org/10.1016/b978-0-08-102491-1.00013-7.

(40) Rouquerol, F.; Rouquerol, J.; Sing, K. S. W.; LLewellyn, P.; Maurin, G.

Adsorption by Powders and Porous Solids; 2014. https://doi.org/10.1016/B978-0-08-097035-6.00007-3.

(41) Lowell, S.; Shields, J. E.; Morral, J. E. *Powder Surface Area and Porosity, 2nd Edition*; 2009; Vol. 107. https://doi.org/10.1115/1.3225796.

(42) State, K.; State, E.; State, K. Langmuir , Freundlich , Temkin and Dubinin – Radushkevich Isotherms Studies of Equilibrium Sorption of Zn 2 + Unto Phosphoric Acid Modified Rice Husk. *IOSR J. Appl. Chem.* **2012**, *3* (1), 38–45. https://doi.org/10.9790/5736-0313845.

(43) de Sá, A.; Abreu, A. S.; Moura, I.; Machado, A. V. *Polymeric Materials for Metal Sorption from Hydric Resources*; Elsevier Inc., 2017. https://doi.org/10.1016/b978-0-12-804300-4.00008-3.

(44) Bruggen, B. Van Der. *Encyclopedia of Membranes*; Springer Berlin Heidelberg, 2015. https://doi.org/10.1007/978-3-642-40872-4.

(45) Bushra, R.; Ahmed, A.; Shahadat, M. *Advanced Environmental Analysis: Applications of Nanomaterials*; Elsevier Inc., 2017; Vol. 2017-Janua. https://doi.org/10.1039/9781782623625-00090.

(46) Sun, J. X.; Sun, X. F.; Zhao, H.; Sun, R. C. Isolation and Characterization of Cellulose from Sugarcane Bagasse. *Polym. Degrad. Stab.* **2004**, *84* (2), 331–339. https://doi.org/10.1016/j.polymdegradstab.2004.02.008.

(47) Worsfold, P. J.; Zagatto, E. A. G. *Spectrophotometry: Overview ☆*, 3rd ed.; Elsevier Inc., 2017. https://doi.org/10.1016/b978-0-12-409547-2.14265-9.

(48) Pavia, D. L.; Lampman, G. M.; Kriz, G. S.; Vyvyan, J. R. *Introduction to Spectroscopy*, 4th ed.; Washington, 2009.

(49) Gómez, C. I. Reconocimiento Molecular de Imidazoles y Pirazoles, 2011.

(50) Facey, G. The Effect of Magic Angle Spinning and High Power 1H Decoupling on 13C Cross Polarization NMR Experiments http://u-of-o-nmr-facility.blogspot.com/2009/01/effect-of-magic-angle-spinning-and-high.html (accessed Dec 8, 2019).

(51) UMA. Espectroscopía Fotoelectrónica de Rayos X http://www.scai.uma.es/areas/aqcm/xps/xps.html (accessed Nov 20, 2019).

(52) Dollase, W. A. *Solid State Chemistry and Its Applications by A. R. West* ; 1985; Vol. 41. https://doi.org/10.1107/s0108768185002476.

(53) Gabriel Tuesta, E.; Huaypar Vásquez, Y. *Aplicación De La Técnica De Difracción De Rayos X (DRX) En La Industria Minera*; 2012.

(54) Segal, L.; Creely, J. . J.; Martin, A. E.; Conrad, C. M. Empirical Method for Estimating the Degree of Crystallinity of Native Cellulose Using the X-Ray Diffractometer. **1958**, 786–794.

(55) Materials Evaluation and Engineering, I. Scanning Electron Microscopy | SEM Failure Analysis | SEM Material Analysis https://www.mee-inc.com/hamm/scanning-electron-microscopy-sem/ (accessed Mar 4, 2020).

(56) Arenas-Lago, D.; Rodríguez-Seijo, A.; Andrade Couce, L.; Vega, F. A. *Multianalytical Approach for the Assessment of Toxic Element Distribution in Soils from Mine and Quarry Areas*; Elsevier Inc., 2017. https://doi.org/10.1016/B978-0-12-809588-1.00002-5.

(57) Materials Evaluation and Engineering, I. Energy Dispersive X-Ray Spectroscopy | EDS Failure Analysis | EDS Material Analysis | EDX Failure Analysis | EDX Material Analysis https://www.mee-inc.com/hamm/energy-dispersive-x-ray-spectroscopyeds/ (accessed Mar 4, 2020).

(58) Groenewould, W. *Characterization of Polymers by Electrothermal Analysis*, 1st ed.; Elsevier Science, 2001.

(59) Laboratorio de Técnicas Espectroscópicas (LABTE). Adsorción física de gases http://www.labte.es/index.php/es/2013-11-03-19-54-23/propiedades-texturales/adsorcion-fisica-de-gases (accessed Jan 20, 2020).

(60) Marcilla, A.; Gomez-Siurana, A.; Muñoz, M. J.; Valdés, F. J. Comments on the Methods of Characterization of Textural Properties of Solids from Gas Adsorption Data. *Adsorpt. Sci. Technol.* **2009**, *27* (1), 69–84. https://doi.org/10.1260/026361709788921579.

(61) Sun, R. C.; Fang, J. M.; Tomkinson, J. Delignification of Rye Straw Using Hydrogen Peroxide. *Ind. Crops Prod.* **2000**, *12* (2), 71–83. https://doi.org/10.1016/S0926-6690(00)00039-X.

(62) Bian, J.; Peng, F.; Pai, P.; Xu, F. CELLULOSE FROM SUGARCANE BAGASSE : STRUCTURAL. **2012**, No. August. https://doi.org/10.15376/biores.7.4.4626-4639.

(63) Liu, C. F.; Sun, R. C. *Cellulose*, 1st ed.; Elsevier, 2010. https://doi.org/10.1016/B978-0-444-53234-3.00005-5.

(64) Johar, N.; Ahmad, I.; Dufresne, A. Extraction, Preparation and Characterization of Cellulose Fibres and Nanocrystals from Rice Husk. *Ind. Crops Prod.* **2012**, *37* (1), 93–99. https://doi.org/10.1016/j.indcrop.2011.12.016.

(65) Sasikala, M.; Umapathy, M. J. Preparation and Characterization of Pineapple Leaf Cellulose Nanocrystal Reinforced Gelatin Bio-Nanocomposite with Antibacterial Banana Leaf Extract for Application in Food Packaging. **2018**, 19979–19986. https://doi.org/10.1039/c8nj02973c.

(66) Yang, H.; Yan, R.; Chen, H.; Lee, D. H.; Zheng, C. Characteristics of Hemicellulose, Cellulose and Lignin Pyrolysis. *Fuel* **2007**, *86* (12–13), 1781–1788. https://doi.org/10.1016/j.fuel.2006.12.013.

(67) Umesh P. Agarwal and Rajai H. Atalla; Reflection, A. T. A Vibrational Spectroscopy. **2010**, 103–136. https://doi.org/10.1201/EBK1574444865-c4.

(68) Madhurambal, G.; Mariappan, M.; Ravindran, B.; Mojumdar, S. Thermal and FTIR Spectral Studies in Various Proportions of Urea Thiourea Mixed Crystal. *Therm. Anal. Calorim.* **2011**, *104* (3), 885–891. https://doi.org/10.1007/s10973-011-1290-6.

(69) Xiang, Q.; Lee, Y.; Pettersson, P.; Torget, R. Heterogeneous Aspects of Acid Hydrolysis of A-Cellulose. In *Applied Biochemistry and Biotechnology*; Humana Press, Totowa, NJ, 2003; pp 505–514. https://doi.org/https://doi.org/10.1007/978-1-4612-0057-4_42.

(70) Mohtar, S. S.; Nur, T.; Tengku, Z.; Busu, M.; Noor, A. M.; Shaari, N.; Mat, H. An Ionic Liquid Treatment and Fractionation of Cellulose, Hemicellulose and Lignin from Oil Palm Empty Fruit Bunch. *Carbohydr. Polym.* **2017**. https://doi.org/10.1016/j.carbpol.2017.02.102.

(71) Bismarck, A.; Aranberri-Askargorta, I.; Springer, J. Surface Characterization of Flax , Hemp and Water Uptake Behavior. *Polym. Compos.* **2002**, *23* (5), 872–894. https://doi.org/10.1002/pc.10485.

(72) Guo, J.; Catchmark, J. M. Surface Area and Porosity of Acid Hydrolyzed Cellulose Nanowhiskers and Cellulose Produced by Gluconacetobacter Xylinus. *Carbohydr. Polym.* **2012**, *87* (2), 1026–1037. https://doi.org/10.1016/j.carbpol.2011.07.060.

(73) Trilokesh, C.; Babu Uppuluri, K. Isolation and Characterization of Cellulose Nanocrystals from Jackfruit Peel. *Mater. Lett.* **2014**, *129*, 20–23. https://doi.org/10.1016/j.matlet.2014.05.019.

(74) Wen, X.; Wang, H.; Wei, Y.; Wang, X.; Liu, C. Preparation and Characterization of Cellulose Laurate Ester by Catalyzed Transesterification. *Carbohydr. Polym.* **2017**, *168*, 247–254. https://doi.org/10.1016/j.carbpol.2017.03.074.

(75) Isab, A. A.; Wazeer, M. I. M. Complexation of Zn(II), Cd(II) and Hg(II) with Thiourea and Selenourea: A 1H, 13C, 15N, 77Se and 113Cd Solution and Solid-State NMR Study. *J. Coord. Chem.* **2005**, *58* (6), 529–537. https://doi.org/10.1080/00958970500038951.

(76) Dorez, G.; Ferry, L.; Sonnier, R.; Taguet, A. Journal of Analytical and Applied Pyrolysis Effect of Cellulose , Hemicellulose and Lignin Contents on Pyrolysis and Combustion of Natural Fibers. *J. Anal. Appl. Pyrolysis* **2014**, *107*, 323–331. https://doi.org/10.1016/j.jaap.2014.03.017.

(77) Kok, M. V.; Ozgur, E. Environmental Effects Characterization of Lignocellulose Biomass and Model Compounds by Thermogravimetry. *Energy Sources, Part A Recover. Util. Environ. Eff.* **2017**, *39* (2), 134–139. https://doi.org/10.1080/15567036.2016.1214643.

(78) Morán, J. I.; Alvarez, V. A.; Cyras, V. P.; Vázquez, A. Extraction of Cellulose and Preparation of Nanocellulose from Sisal Fibers. *Cellulose* **2008**, *15* (1), 149–159. https://doi.org/10.1007/s10570-007-9145-9.

(79) Soares, S.; Caminot, G.; Levchik, S. Comparative Study of the Thermal Decomposition of Pure Cellulose and Pulp Paper. *Polym. Degrad. Stab.* **1995**, *49* (2), 275–283.

(80) Wang, S.; Gao, Q.; Wang, J. Thermodynamic Analysis of Decomposition of Thiourea and Thiourea Oxides. *J. Phys. Chem. B* **2005**, *109* (36), 17281–17289. https://doi.org/10.1021/jp051620v.

(81) Park, S.; Baker, J. O.; Himmel, M. E.; Parilla, P. A.; Johnson, D. K. Cellulose Crystallinity Index : Measurement Techniques and Their Impact on Interpreting Cellulase Performance. **2010**, 1–10.

(82) Mohankumara, P. B.; Thakare, S. P.; Guna, V.; Arpitha, G. R. Millettia Pinnata : A Study on the Extraction of Fibers and Reinforced Composites. *Bioresour. Bioprocess.* **2020**, *2*, 3–8. https://doi.org/10.1186/s40643-019-0292-2.

(83) Belgacem, M. N.; Czeremuszkin, G.; Sapieha, S.; Gandini, A. Surface Characterization of Cellulose Fibres by XPS and Inverse Gas Chromatography. *Cellulose* **1995**, *2* (3), 145–157. https://doi.org/10.1007/BF00813015.

(84) Wade, L. G. *Wade Organic Chemistry 8e.Pdf*, 8th ed.; United States of America, 2013.

(85) Moulder, J. F.; Stickle, W. F.; Sobol, P. E.; Bomben, K. D. *Handbook of X-Ray Photoelectron Spectroscopy*; Chastain, J., Ed.; Perkin-Elmer Corporation: United States of America, 1992.

(86) Jiao, C.; Zhang, Z.; Tao, J.; Zhang, D.; Chen, Y.; Lin, H. Synthesis of a Poly(Amidoxime-Hydroxamic Acid) Cellulose Derivative and Its Application in Heavy Metal Ion Removal. *RSC Adv.* **2017**, *7* (44), 27787–27795. https://doi.org/10.1039/c7ra03365f.

(87) Yu, Z.; Bai, Y.; Wang, Y.; Liu, Y.; Zhao, Y.; Liu, Y.; Sun, K. One-Step Synthesis of Three-Dimensional Nitrogen and Sulfur Co-Doped Graphene Networks as Low Cost Metal-Free Counter Electrodes for Dye-Sensitized Solar Cells. *Chem. Eng. J.* **2017**, *311*, 302–309. https://doi.org/10.1016/j.cej.2016.11.093.

(88) Dong, Y.; Pang, H.; Yang, H. Bin; Guo, C.; Shao, J.; Chi, Y.; Li, C. M.; Yu, T. Carbon-Based Dots Co-Doped with Nitrogen and Sulfur for High Quantum Yield and Excitation-Independent Emission. *Angew. Chemie - Int. Ed.* **2013**, *52* (30), 7800–7804. https://doi.org/10.1002/anie.201301114.

(89) Man, H. C.; Chin, W. H.; Zadeh, M. R.; Yusof, M. R. M. Adsorption Potential of Unmodified Rice Husk for Boron Removal. *BioResources* **2012**, *7* (3), 3810–3822. https://doi.org/10.15376/biores.7.3.3810-3822.

(90) Huheey, J.; Keiter, E.; Keiter, R. *Inorganic Chemistry: Principles of Structure and Reactivity*, 4th ed.; 1973; Vol. 50. https://doi.org/10.1021/ed050pa379.1.

(91) IWA. Filtration Processes | IWA Publishing https://www.iwapublishing.com/news/filtration-processes (accessed Mar 4, 2020).

(92) Miller, J. N.; Miller, J. C. *Statistics and Chemometrics for Analytical Chemistry*, 6th ed.; Pearson Education Limited, 2010.